Tail bud progenitor activity relies on a network comprising *Gdf11*, *Lin28* and *Hox13* genes.

Rita Aires[1], Luisa de Lemos[1], Ana Nóvoa[1], Arnon Dias Jurberg[1,#], Bénédicte Mascrez[2], Denis Duboule[2,3], Moisés Mallo[1]*

1 Instituto Gulbenkian de Ciencia, Rua da Quinta Grande 6, 2780-156 Oeiras, Portugal

2 Department of Genetics and Evolution, University of Geneva, Sciences III, 1211 Geneva 4, Switzerland

3 School of Life Sciences, Ecole Polytechnique Federale, 1015 Lausanne, Switzerland

Current address: Laboratory on Thymus Research, Oswaldo Cruz Institute, Oswaldo Cruz Foundation/Fiocruz, Av. Brasil, 4365. Pavilhão Leônidas Deane, Manguinhos, Rio de Janeiro-RJ, Brazil. 21040-360.

* Corresponding and lead author: e-mail: mallo@igc.gulbenkian.pt

Keywords: Axial progenitors; vertebrate; axial extension; tail bud; Gdf11; Lin28; Hoxb13; Hoxc13

ABSTRACT

During the trunk to tail transition axial progenitors relocate from the epiblast to the tail bud. Here, we show that this process entails a major regulatory switch, bringing tail bud progenitors under Gdf11 signaling control. *Gdf11* mutant embryos have an increased number of such progenitors that favor neural differentiation routes, resulting in a dramatic expansion of the neural tube. Moreover, inhibition of Gdf11 signaling recovers the proliferation ability of these progenitors when cultured *in vitro*. Tail bud progenitor growth is independent of *Oct4*, relying instead on *Lin28* activity. Gdf11 signaling eventually activates *Hox* genes of paralog group 13, which halt expansion of these progenitors, at least in part by down-regulating Lin28 genes. Our results uncover a genetic network involving *Gdf11*, *Lin28* and *Hox13* genes controlling axial progenitor activity in the tail bud.

INTRODUCTION

The vertebrate body is progressively laid down during embryonic development in an anterior to posterior sequence along its main axis. This process relies on the activity of distinct cell populations, collectively known as axial progenitors (Aires et al., 2018; Stern et al., 2006; Wilson et al., 2009). At early developmental stages, these progenitors are located in the epiblast, an epithelial layer that, as the embryo develops, gets restricted to its posterior end and becomes contiguous with the developing central nervous system (Psychoyos and Stern, 1996; Wilson and Beddington, 1996). These epiblast-resident progenitors extend the post-cranial body axis all the way from the head through the trunk regions. However, as the epiblast recedes, axial progenitors relocate to the tail bud from where they further elongate the body by generating tail tissues (Aires et al., 2018; Wilson et al., 2009). In recent years, efforts have been directed towards both the characterization of these progenitors, as well as to understanding how their activity is regulated. Among the various subsets of progenitors, most of the attention has been drawn by the so-called neuro-mesodermal progenitor (NMP) (Aires et al., 2018; Henrique et al., 2015; Steventon and Martinez Arias, 2017). Grafting experiments and clonal analyses

revealed their dual potency in the generation of both the spinal cord and paraxial mesoderm of the trunk and tail regions (Cambray and Wilson, 2007, 2002; Tzouanacou et al., 2009). These cells are typically identified by the co-expression of Sox2 and T(Brachyury) [$Sox2^{+}$/$T(Bra)^{+}$], neural and mesodermal markers respectively, on the basis of their expression profiles in regions known to contain NMPs (Cambray and Wilson, 2007; Wymeersch et al., 2016).

Several signaling pathways and transcription factors have been shown to play relevant roles in the control of NMP growth, maintenance and differentiation along neural or mesodermal lineages. FGF and Wnt signaling are amongst the most important. Simultaneous inactivation of *Fgf4* and *Fgf8* in the mouse results in strong axial truncations due to a drastic reduction of axial progenitors (Boulet and Capecchi, 2012; Naiche et al., 2011). Likewise, *Wnt3a* inactivation also causes truncations at the trunk level, indicating its requirement for NMP activity (Greco et al., 1996; Takada et al., 1994). *Wnt3a*, however, also controls NMP differentiation, both by blocking neural determination and by promoting mesodermal fates together with *Tbx6* (Garriock et al., 2015; Gouti et al., 2014; Jurberg et al., 2014; Martin and Kimelman, 2008; Takemoto et al., 2011; Tsakiridis et al., 2014). *T/Brachyury* and the *Cdx* gene family are also essential for normal NMP function. Absence of these factors in the mouse truncates the embryo after the first few somites, which coincides with the beginning of NMP contribution to axial extension (Herrmann et al., 1990; Savory et al., 2011).

Clonal analyses in the mouse indicate that NMPs are a continuous cell population throughout axial extension and are involved in the formation of the neural tube and paraxial mesoderm at all post-cranial axial levels (Tzouanacou et al., 2009). However, a variety of data indicate that the intrinsic properties of NMPs differ depending on their position along the anterior-posterior body axis. The most striking example is neural tube formation: while trunk NMPs make this structure by primary neurulation, their tail counterparts generate it by secondary neurulation (Schoenwolf and Smith, 1990). The fate of these two sections of the neural tube is different too, as most mature spinal cord derives from trunk neural tube whereas the secondary neural tube is mostly eliminated during the final stages of embryonic development (Nievelstein et al., 1993). Paraxial mesoderm formation and somitogenesis also have distinct mechanistic

requirements whether they derive from epiblast- or tail bud-residing NMPs. Indeed, it has been observed a differential requirement for the cycling behavior of *Lfng* expression (Shifley et al., 2008; Williams et al., 2014), as well as distinctive sensitivities to the presence of *Hoxb6* activity (Casaca et al., 2016) at trunk or tail axial levels.

The molecular bases underlying these differences are elusive. *Oct4* seems to be one of the factors involved in generating functional differences between epiblast and tail bud progenitors, as its activity is essential for trunk development but dispensable during tail-forming stages (Aires et al., 2016; DeVeale et al., 2013). It is therefore possible that equivalent factors exist to control tail bud NMP activity, although potential candidates for such roles have yet to be discovered. Genetic studies have identified some genes that seem to affect axial extension specifically at the level of the trunk to tail transition (Abu-Abed et al., 2001; Ho et al., 2012; Sakai et al., 2001; Yamaguchi et al., 1999). However, inactivation of these factors often leads to strong axial truncations at that particular axial level, which complicates the study of their contribution to tail bud NMP activity. Due to the cumulative nature of embryonic development, severe truncations in the tail could as well derive from a critical role in the control of the trunk to tail transition, rather than from a direct involvement of the same factors in the regulation of tail bud-resident progenitors. *Gdf11* seems to come out as an exception amongst these genes. Despite its central role in the control of the trunk to tail transition (Jurberg et al., 2013), its activity in this process is partially compensated by *Gdf8* (McPherron et al., 2009), thus allowing the onset of tail development in *Gdf11* mutant mice. Interestingly, tails of *Gdf11* mutant fetuses display morphological differences to those of wild type embryos (Lee et al., 2010), suggesting an additional role for this signaling molecule in the regulation of tail bud progenitor activity.

Here, we show that Gdf11 signaling is involved in the control of tail bud NMP activity. We found that the tail bud NMP population is expanded in *Gdf11* mutant embryos and that their differentiation becomes biased towards the production of neural tissues. This activity can also be seen *in vitro*, as tail bud progenitors proliferate considerably in culture when Gdf11 signaling is inhibited. Interestingly, this growth is independent of *Oct4*. Instead, our data indicate that *Lin28* genes take a prominent role in the proliferation of axial progenitors after

the trunk to tail transition. Lin28 activity is then negatively regulated by *Hox* genes of the paralog group 13 (most specifically *Hoxb13* and *Hoxc13*), which in the mouse are activated by Gdf11 signaling at the final stages of tail development. Our results indicate that epiblast and tail bud NMPs are under the control of different regulatory mechanisms and uncover a genetic network involving *Gdf11*, *Lin28* and *Hox13* genes regulating the activity of these progenitors after they have relocated to the tail bud.

RESULTS

Tail malformations in *Gdf11* mutant embryos

Skeletal preparations at embryonic day (E) 18.5 embryos showed clear differences in the post-sacral region of *Gdf11* mutant fetuses when compared to wild type littermates (Fig. 1A). Despite some variation between specimens, tails of *Gdf11*$^{-/-}$ fetuses were always composed of vertebrae with fully developed neural arches accommodating neural tube until their very posterior end (Fig. 1Ae, Af). This contrasted with the tail anatomy of wild type embryos, where caudal vertebrae lacked neural arches after their fourth element, coincident with the end of the neural tube (Fig. 1Ab, Ac).

Abnormalities in *Gdf11*$^{-/-}$ tail development were already visible as early as E10.5. In mutant embryos, the tail did not show the typical tapering observed in wild type embryos (Fig. 1Bd) and frequently displayed tail bifurcations (Jurberg et al., 2013; and not shown). The transversal area at the level of the presomitic mesoderm (PSM) was 64% larger in *Gdf11* mutants than in their wild type littermates (Fig. 1Bf and1C). Histological analyses (Fig. 1B) revealed equivalent tissue compositions in wild type and *Gdf11*$^{-/-}$ embryos, comprised of a dorso-medial neural tube, delimited laterally by paraxial mesoderm and ventrally by the notochord and tail endoderm. *Gdf11* mutants also exhibited an ectopic ventral mass, which we had previously proposed might result from incomplete epiblast regression (Aires et al., 2016) (Fig.1Be, Bf, asterisk). However, despite their global similar histological structure, there were substantial quantitative divergences between wild type and *Gdf11*$^{-/-}$ embryos.

The most striking difference was the dramatic increase in neural tube area, which was about three-fold larger in *Gdf11* mutant embryos (Fig. 1B, D). Tail gut also occupied a broader area in *Gdf11* mutants, although part of this

difference could stem from the invasion of the gut lumen by the ectopic ventral mass (Fig. 1Be, Bf). The presence of the ectopic pocket complicated precise quantification of the mesoderm, as this structure contains a significant mesenchymal component rich in mesodermal marker expression (Fig. S1). When this ectopic pocket was taken into account, the area occupied by mesodermal tissues was increased by about 25% in *Gdf11*$^{-/-}$. However, when the ectopic mass was excluded from the analysis, the mesodermal tissue contribution, essentially represented by the paraxial mesoderm, was not significantly different in wild type and *Gdf11* mutant embryos (Fig. 1D). These results indicate that the extended spinal cord observed in the tail of E18.5 *Gdf11* mutant embryos most likely derives from excessive formation of neural tissue during tail extension. Noteworthy, the different structural characteristics of the associated vertebrae do not appear to require formation of extra paraxial mesoderm, suggesting that they might have been produced during somite differentiation.

Gdf11 mutant embryos contain expanded numbers of tail bud NMPs

Axial extension at tail stage is powered by the activity of tail bud-resident NMPs (Henrique et al., 2015). It is thus possible that the observed structural defects in *Gdf11* mutant tails originate from defective regulation of NMP number and/or fate. Fluorescence activated cell sorting (FACS) analyses of tail bud cells from E10.5 wild type and mutant embryos using antibodies against Sox2 and T(Bra) revealed complex two-dimensional patterns of continuous expression, rather than discreet populations (Fig. 2A). These patterns most probably reflect the process of lineage commitment, in which the NMPs [Sox2^{+}/T (Bra)$^{+}$] and their progeny gradually take a more neural (Sox2^{+}) or mesodermal [T(Bra)$^{+}$] fate as the tail elongates, without immediately loosing expression of the other marker gene. The patterns obtained from *Gdf11*$^{-/-}$ tails were consistently different to those of wild type embryos, including an increase in the total proportion of Sox2^{+}/T(Bra)$^{+}$ cells of about 23%, particularly regarding low-to-moderate Sox2 and T expression levels (Fig. 2A, B). As NMPs might belong to the cell pool expressing moderate levels of both markers (Wymeersch et al., 2016), it is possible that this differential cell distribution in the tails of *Gdf11* mutants reflects a genuine, although moderate, enrichment in tail NMPs.

The FACS profiles also revealed that, despite some variability, *Gdf11* mutant tail buds, contained almost twice as many $Sox2^{+}$ cells, along with a 37% decrease in the proportion of T-expressing cells when compared with their wild type littermates (Fig. 2B). These results suggest a general bias in NMP differentiation favoring the production of neural derivatives in the absence of Gdf11 signaling. This is consistent with the proportionally larger neural tubes observed in *Gdf11* mutant embryos.

We further evaluated both the NMP content of wild type and *Gdf11* mutant embryos and their differentiation patterns using a genetic lineage-tracing scheme that combines the *Cdx2-Cre*^{ERT} transgenic mice, which express the tamoxifen-inducible Cre^{ERT} recombinase in axial progenitors throughout development (Jurberg et al., 2013; Jurberg et al., 2014), with the *ROSA26r-β-gal* reporter (Soriano, 1999). Administering a single low tamoxifen dose to pregnant females carrying embryos with the *ROSA26r- β-gal*$^{+/0}$::*Cdx2-Cre*$^{ERT(+/0)}$ genotype at E7.5 labels NMPs permanently with *β*-gal at the stage when these cells are engaged in neck/upper thoracic region development. Under such low dosage conditions, recombination is effective in a reduced number of cells for approximately 8 hours (Danielian et al., 1998) and, therefore, any *β*-gal-positive cell identified a few days later at more caudal embryonic levels must derive from this pulse of labeled NMPs. Successful NMP labeling was confirmed by the presence of *β*-gal-positive cells in neural and mesodermal derivatives all along the body axis caudal to the forelimb bud in E10.5 embryos (Fig. 3A). Importantly, we also found stained cells in the tail bud of these embryos, which included the chordo-neural hinge (Fig. 3Aa''), consistent with NMPs being a continuous cell population as previously reported (Tzouanacou et al., 2009).

The total number of β-gal-labeled cells per embryo showed some heterogeneity in both wild type and *Gdf11*$^{-/-}$ embryos, most likely due to variability in tamoxifen-induced Cre recombination. However, the general staining patterns, as well as the ratio of cells contributing to neural and mesodermal tissues were consistent amongst experiments. We detected equivalent ratios of labeled cells in sections at trunk levels of wild type and *Gdf11* mutants with a similar distribution between neural and mesodermal derivatives (Fig. 3A, B). These results indicate that the absence of Gdf11

signaling did not produce a bias in the differentiation fate of these progenitors during trunk development.

In contrast, while in the tails of *Gdf11* mutants the contribution of β-gal-labeled cells to neural tissues was similar to that observed at trunk regions, it was reduced by 60% in wild type embryos (Fig. 3C). A similar trend was observed in the mesodermal components of the tail, although not as strikingly, most particularly if the ectopic epithelial pocket is considered. Indeed, a considerable part of the β-gal^{+} cells accumulated in the ectopic ventral mass, including both its epithelial and mesenchymal components (Fig. 3Ab, Ab'', D). This is consistent with the epithelial component of this mass being a remnant of the epiblast, still producing mesodermal derivatives that accumulate within the epithelial pocket (Aires et al., 2016). In addition, to the increased global numbers of labeled cells in the tails of *Gdf11* mutant embryos, the proportion of these cells found in neural structures was consistently higher in the *Gdf11*$^{-/-}$ than in wild type tails (Fig. 3B-D). In particular, while in the tails of wild type embryos the frequency of labeled cells found in neural structures was similar to that observed at trunk levels (approximately 8%), in *Gdf11*$^{-/-}$ embryos about 13% of the labeled cells was found in the neural tube (Fig. 3D). These results are in agreement with the three-fold increase of the neural tube area found in mutant embryonic tails and indicate an increased contribution of progenitors to neural lineages in the absence of Gdf11 signaling. Yet, a differential increase in proliferation rates could also contribute to the expanded tail bud neural derivatives in the absence of Gdf11 signaling. Indeed, we observed an approximate two-fold increase in proliferation specifically in the neural tubes of *Gdf11* mutants (Fig. 3 E, F). Interestingly, we found a small reduction of proliferating cells in mesodermal compartments (including both paraxial mesoderm and ectopic ventral mass) of *Gdf11* mutant tails. This could explain the decrease in the contribution of β-gal^{+} cells to the paraxial mesoderm, even if there are seemingly more mesodermal progenitors transitioning to the tail (Fig. 3D).

Together, these results show that Gdf11 signaling affects tail bud NMPs in at least two distinct ways. First, *Gdf11* seems to control the overall number of those progenitors, as part of the reorganization of the progenitor pool during the trunk to tail transition and during extension throughout the tail. Secondly, it

appears to affect their fate decisions by restricting their contribution to neural lineages.

Tail bud explants grow *in vitro* in the absence of Gdf11 signaling

The experiments reported above indicate that NMP growth properties may be under different regulation before and after the trunk to tail transition. Axial progenitors have been shown to lose their ability to grow *in vitro* at around E9.0, approximately coincident with their relocation to the tail bud (Osorno et al., 2012). As the NMP tail bud population seemed to be expanded in *Gdf11* mutant embryos, we hypothesized that Gdf11 signaling could be involved in arresting the growth of these cells *in vitro*. We tested this by comparing the growth of tail bud cells explanted from either wild type or *Gdf11* mutant E10.5 embryos in culture conditions known to facilitate NMP production (Gouti et al., 2014). Cells obtained from wild type embryos were maintained in culture for several days and were able to withstand at least three passages. However these cells expanded slowly, with an average population doubling time (PDT) of 57h, until they gradually lost the ability to grow and eventually died within 15 to 18 days (Fig. 4A), consistent with previously published observations (Osorno et al., 2012).

In contrast, cells derived from *Gdf11*$^{-/-}$ embryos had a decreased PDT (≈29h) and sustained steady growth during several passages, although the population doubling levels were somewhat variable amongst experiments (Fig. 4A). This variation could reflect heterogeneity of the explanted cells and/or partial replacement of the Gdf11 activity by Gdf8 or components of the growth media. To block such potential interferences, we incubated *Gdf11* mutant tail bud cells in the presence of SB431542, an inhibitor of Alk5 (also known as TgfβRI), which is the type I receptor mediating Gdf11 activity (Andersson et al., 2006). This treatment not only increased the overall growth capacity of the cells by decreasing the PDT to ≈18h, but also reduced the experimental variability (Fig. 4A). Interestingly, SB431542 could rescue the growth ability of wild type tail bud cells to levels similar to those obtained with *Gdf11* mutant cells cultured under similar conditions (PDT ≈21h) (Fig. 4A). These results are consistent with our *in vivo* observations, supporting a role for *Gdf11* signaling in the control of the growth properties of tail bud-derived progenitors.

Gene expression analyses for neural and mesodermal marker genes at 3, 6 and 9 days post-culture confirmed that the absence of Gdf11 signaling promotes neural fates *in vitro*. *Gdf11*$^{-/-}$ tail buds, as well as mutant and wild type explants cultured with SB431542 expressed Sox2, Tubulin and Nestin (Fig. 4B, C and Fig.S2A, B), while these genes were down regulated or even not detected in wild type cultures. Conversely, mesodermal markers such as *T (Bra)* and *Mesogenin1* were activated in wild type cells before they were switched off (Fig. 4B and Fig S2A). Interestingly, we found some cells co-expressing Sox2 and T (Bra) at day 3 post-plating, particularly in Gdf11-deficient conditions. However these cells quickly disappeared in the following passage, which agrees with the transitory nature of Sox2^{+}/T (Bra)$^{+}$ cells in culture (Gouti et al., 2014). *Tbx6* expression, however, stood out amongst the tested mesodermal markers, as it showed slight and variable increase in the absence of Gdf11 signaling. In particular, Tbx6 was frequently observed in combination with Sox2 (Fig. 4B and Fig. S2C). This behavior might be related to an increased and transitory presence of tail bud NMPs in those cultures, since *Tbx6* expression has been recently linked to tail bud NMPs (Javali et al., 2017). Together, these results suggest that *in vitro* tail bud explant cultures can mimic the effects of the absence of Gdf11 signaling we had observed *in vivo*.

It has been shown that *Oct4* can recover tail bud cell growth *in vitro* (Osorno et al., 2012), thus opening the possibility that inhibition of Gdf11 signaling might produce *de novo Oct4* activation in explanted cells, which in turn would promote their proliferation. However, we consider it unlikely, as we were unable to detect *Oct4* expression in cultured cells (not shown). This observation suggests that tail bud cell proliferation must be regulated by mechanisms different from those operating on their epiblast-located counterparts, thus supporting the hypothesis that epiblast and tail bud NMPs are functionally distinct cell populations.

Differential gene expression in *Gdf11* mutant tails

To assess how Gdf11 regulates tail bud NMP activity, we compared the RNA profiles of E10.5 wild type and *Gdf11*$^{-/-}$ tail buds by RNA-seq (Table S1). Gene ontology analysis for the top 88 genes that showed an increase of two or more fold in *Gdf11*$^{-/-}$ tails revealed substantial enrichment in genes involved in the

positive regulation of neuroblast development, neural cell migration, and kidney and limb development (Fig. S3A). Induction of both hind limbs and kidneys is closely associated with the region of the trunk to tail transition; therefore, the increased expression levels of genes related to these structures might be linked to the delay of this transition in *Gdf11*$^{-/-}$ embryos. Expression of factors involved in neural tube development and neural stem cell function were also up regulated in mutant embryos (Fig. 5A), consistent with their considerably larger neural tubes.

Conversely, *T (Bra)*, *Tbx6* and *Mesogenin1*, commonly associated with mesodermal fates, were found down-regulated in these embryos (Fig. 5A, Fig. S3B). *In situ* hybridization analyses confirmed that in *Gdf11*$^{-/-}$ embryos, expression of these genes was reduced in the tail PSM, although their expression was still significant in the ectopic mass (Fig. S1). These results corroborate the NMP differentiation bias towards neural fates in the tail bud of *Gdf11* mutant embryos, as already indicated by the FACS analyses and cell tracing experiments. It should be noted that despite its reduction in size, the PSM of *Gdf11* mutant embryos preserved cycling activity (Fig. S1D), which is consistent with the production of individual vertebral units in the area caudal to the hind limbs. Interestingly, expression of *Sox10*, a gene associated with neural crest (Southard-Smith et al., 1998), was substantially higher in the *Gdf11* mutant dataset (Fig. 5A). *In situ* hybridization analyses showed that in the mutant embryos neural crest cell production covered almost the whole extent of the neural tube, in contrast with wild type embryos that lacked neural crest derivatives in most of their tail region (Fig. S3D).

Out of these many differentially expressed genes (Fig. 5A), we particularly focused on the *Lin28* genes, which code for RNA binding proteins involved in the maturation of several miRNAs, most prominently those of the let-7 family (Viswanathan and Daley, 2010). These genes are interesting in the context of axial progenitor activity due to their association with the expansion of neural progenitors (Yang et al., 2015) and their link to a metabolic pathway that seems to play a relevant role in the expansion of tail bud progenitors (Oginuma et al., 2017; Zhu et al., 2011). *Lin28a* is expressed in the tail bud of E10.5 wild type embryos, particularly in the progenitor-residing areas, the caudal part of the neural tube and adjacent ventral mesoderm (Fig. 5Ba and Fig. S3Ea). One

day later, this gene becomes strongly down-regulated in the entire tail region (Fig. 5Bi and Fig. S3Ec). *Lin28a* expression in E10.5 *Gdf11* mutants grossly resembled the pattern observed in wild type embryos, although the signal in the tail bud appeared stronger (Fig. 5Be and Fig. S3Eb). This was consistent with RNA-seq data, which showed an almost two-fold increase in expression relative to wild type tail buds (Fig. 5A). However, *Lin28a* remained robustly expressed in the tails of E11.5 *Gdf11*$^{-/-}$ embryos (Fig. 5Bm and Fig. S3Ed), indicating that *Lin28a* may participate in the tail phenotype exhibited by *Gdf11* mutants. Equivalent patterns were observed with *Lin28b* (Fig. 5Bb, Bf, Bj, Bn). Notably, expression of both *Lin28a* and *Lin28b* was distinctly strong in *Gdf11* mutant embryos, in their posterior neural tube and in the progenitor-containing region of the tail bud at E11.5, which contrasted with the absence of any detectable transcripts for these genes in the same regions of wild type embryos at this developmental stage.

We then tested the effect of sustained *Lin28 gene* expression in axial progenitors by expressing *Lin28a* and *Lin28b*, either alone or in combination, using the *Cdx2* enhancer. At E18.5, transgenic fetuses had longer tails, with a significant increase in number of caudal vertebrae (Fig. 5C). In addition, expression analyses at E13.5, which corresponds to the final stages of axial extension, showed that *T (Bra)* and *Sox2* not only were still present in *Cdx2-Lin28a* transgenic tail buds, but had expanded expression domains (Fig. 5E). Interestingly, some of these *Cdx2-Lin28a* embryos displayed bifurcated tail buds that likely reflected an excessive tail tissue production (Fig. 5Eb, Ee).

Hox13 genes act downstream of Gdf11

RNA-seq datasets also revealed that *Hoxb13* and *Hoxc13* were the most strongly down-regulated genes in *Gdf11*$^{-/-}$ tail buds (Fig. 5A). This differential expression was confirmed by *in situ* hybridization (Fig. 5Bc, Bd, Bg, Bh, Bk, Bl, Bo, Bp). At E10.5, we could not detect any *Hoxb13* and only a faint *Hoxc13* expression in *Gdf11*$^{-/-}$ tails, whereas only residual expression was scored at E11.5. The tails of both *Hoxb13* and *Hoxc13* mutant embryos share some of the abnormal characteristics found in *Gdf11* mutants, although milder in intensity. In particular, *Hoxb13* mutants have thicker, caudally-elongated neural tubes and supernumerary dorsal root ganglia, together with the presence of lateral

processes in a larger number of caudal vertebrae (Economides et al., 2003). *Hoxc13* mutants have not been characterized in so much detail but they also contain a larger number of caudal vertebrae with lateral processes (Godwin and Capecchi, 1998). It is thus possible that these genes are downstream mediators of the Gdf11 activity promoting axial termination.

We thus examined the effect of premature expression of either *Hoxb13* or *Hoxc13* in axial progenitors. Both *Cdx2-Hoxb13* and *Cdx2-Hoxc13* transgenic embryos showed strong underdevelopment of axial structures derived from the tail bud (Fig. 6A-C), which is consistent with previously published data (Young et al., 2009). Molecular analyses of the transgenic embryos at mid-gestation indicated disorganized mesoderm and undersized neural tubes in the tail region, as revealed by *T (Bra)* and *Sox2 in situ* hybridization, respectively (Fig. 6D-I). In addition, we observed a significant decrease in cell proliferation and an increase in apoptotic figures in the posterior end of the neural tube in *Cdx2-Hoxb13* transgenic embryos (Fig. 6O-S). This suggests a specific role for *Hoxb13* during tail development, by restricting cell proliferation and regulating cell death in tail tissues, particularly in the neural tube.

Surprisingly, even in those *Hox13* transgenic embryos showing very strong axial malformations, these alterations were mostly restricted to the tail and only minor (if any) malformations were scored in more anterior embryonic areas despite a strong *Cdx2* enhancer activity in these regions (Fig. 6 A-L). This observation suggests that trunk axial progenitors may be differentially affected by the activity of these *Hox* genes, once again raising the matter of potential differences existing between trunk and tail axial progenitors.

Functional interaction between *Lin28* and *Hox13* genes

A close evaluation of *Lin28* and *Hoxb13* and *Hoxc13* expression patterns in the embryonic tail indicated that they are to some extent inversely correlated (compare Fig. 5Bi and Bk, inlets), suggesting a potential functional association. Consistent with this hypothesis, expression analyses of E10.5 *Cdx2-Hoxb13* and *Cdx2-Hoxc13* transgenic embryos revealed strong *Lin28a* down-regulation (Fig. 6J-L). Since embryos lacking the whole *HoxC* cluster (*HoxCΔ*) display tail alterations similar to those observed with the *Hoxc13* mutant mice (Godwin and Capecchi, 1998; Suemori and Noguchi, 2000) and also to avoid compensation

by other genes from the *HoxC* cluster, we used them as a proxy for *Hoxc13* inactivation in this posterior area. *In situ* hybridization analyses at E10.5 revealed a slight but consistent increase in *Lin28a* expression in *HoxCΔ* when compared to wild type littermates (Fig. 6M, N), further supporting a genetic interaction between *Hox13* and *Lin28* genes.

We also observed an regulated expression of both *Lin28a* and *Lin28b* in explanted tail bud progenitors grown under Gdf11-inhibiting conditions, but not in wild type cells grown in the absence of SB431542 (Fig. 7A, B). The inverse pattern was observed for *Hoxb13* and *Hoxc13* expression, which was activated in wild type cells cultured in the absence of the drug but barely detectable in explanted cells lacking active Gdf11 signaling (Fig. 7A, B and Fig. S4). These results further support a functional interaction between *Lin28* and *Hox13* genes in tail bud progenitors and a key role for Gdf11 signaling in the modulation of this interaction, perhaps through the control of *Hox13* activation. In addition, they indicate that the explanted cells conserve, to a significant extent, most of their *in vivo* properties, particularly regarding the control of cell proliferation.

DISCUSSION

In this work, we propose that the functional characteristics of tail bud axial progenitors and the genetic mechanisms involved in their regulation are different from those operating in their epiblast-resident counterparts. Our data indicates that a genetic network involving *Gdf11*, *Lin28* and *Hox13* genes (most particularly those of the *HoxB* and *HoxC* clusters) is at the core of the mechanisms regulating tail bud NMP activity. This contrasts with the dependence of epiblast axial progenitors on *Oct4* (Aires et al., 2016; DeVeale et al., 2013). This regulatory switch might underlie the differences between trunk and tail NMPs in what concerns both their intrinsic behavior and the fate of their derivatives. The most relevant of those differences involves the neural tube, formed by primary neurulation at trunk levels and by secondary neurulation in the tail (Schoenwolf and Smith, 1990). In the newborn, the spinal cord mostly derives from the primary neural tube, whereas the secondary neural tube is largely eliminated at later developmental stages, contributing very little to adult tissues. Thus, this variation in the mode of neural tube development is not just

purely conceptual, but might actually reflect important underlying differences that are then translated specifically into the neural tube fate.

The tail bud regulatory network might control development of the tail axial progenitors at different stages of their activity during the morphogenesis of tail structures, in which *Lin28* and *Hox13* genes would be mostly associated with activating and repressing processes, respectively. This way, Gdf11 signaling would potentially function as a coordinating unit by controlling the timing of the trunk to tail transition and, therefore, the temporal and mechanistic shift from the molecular networks controlling epiblast-residing progenitors to the ones regulating tail bud-dependent axial extension.

Gdf11 as a regulator of NMP reorganization and expansion during the trunk to tail transition

The first stage in this mechanistic shift might involve regulating the expansion of the tail bud NMPs themselves. The transient nature of these progenitors complicates proper estimation of this variable. However, a variety of observations provide indirect support for this possibility. In particular, forced *Lin28* expression in the progenitor-containing region of the embryo consistently increased the number of tail vertebrae, suggesting a positive effect of these genes on tail bud NMP activity. Conversely, premature expression of *Hoxb13* or *Hoxc13* restricted NMP expansion, leading to strong axial truncations. The increased number of caudal vertebrae in *Hoxb13* mutant embryos (Economides et al., 2003) is also consistent with negative regulation of NMP expansion or maintenance by *Hox13* genes. Finally, the tail bud of *Gdf11*$^{-/-}$ embryos, where *Lin28* activity prevails over *Hox13* genes, contain more Sox2^{+}/T (Bra)$^{+}$ cells, which could reflect enrichment in NMPs.

Interestingly, premature expression of *Hoxb13* and *Hoxc13* in axial progenitors interfered strongly with tail development but had negligible effects on trunk extension, despite robust activity at both axial levels of the *Cdx2* enhancer used in those transgenic experiments. These observations indicate that although NMPs seem to be a continuous cell population throughout the main body axis (Tzouanacou et al., 2009), their functional properties undergo major changes during the process of relocation into the tail bud.

Gdf11 controls neural progenitors during axial extension of the tail

A variety of data indicate that the *Gdf11*/*Lin28*/*Hox13* network also plays a prominent role in the development of the tail-associated neural tube. Cell tracing experiments revealed a higher relative contribution of labeled cells to neural tissues in the tail region of *Gdf11* mutant embryos both when compared to the same region of their wild type littermates and, most importantly, to trunk areas of the same embryo. The observed increase in the mitotic numbers in the tail neural tube of *Gdf11* mutant embryos suggests that differential expansion of the neural progenitors might contribute to this effect. As a consequence, *Gdf11* mutant embryos contained enlarged spinal cords, already evident at early stages of tail development. The remarkable growth capacity of tail bud cell explants grown *in vitro* under Gdf11-deficient conditions, together with their differentiation bias towards neural fates, is consistent with a substantial expansion of a neural progenitor compartment in those cultures. An increase in neural progenitors in *Gdf11* mutant embryos has also been observed during differentiation processes both in the spinal cord (Shi and Liu, 2011) and in the olfactory epithelium (Gokoffski et al., 2011), indicating a general role for *Gdf11* in the control of the neural progenitor pool size during development.

Despite this conservation, the mechanisms associated with Gdf11 activity might differ in the various embryonic areas. In the particular case of tail extension it most likely includes control of *Lin28* and *Hox13* activities. *Lin28* genes, which have been shown to be involved in neural progenitor expansion (Yang et al., 2015), are very highly expressed both in the enlarged tail neural tube of *Gdf11* mutant embryos and in cultured tail bud explants incubated under Gdf11 inhibiting conditions. This expression contrasts with the normal dynamics of *Lin28* expression in the developing tail, where it becomes progressively reduced coincident with the decrease in tail neural tube size. *Lin28* expression levels are also very low or absent in tail bud cell explants cultured under Gdf11-permissive conditions. The increased *Sox2* expression in the posterior end of the tail of E13.5 *Cdx2-Lin28a* transgenic embryos provides additional support for the competence of *Lin28* genes to promote neural fates in the tail bud. In addition, the inverse correlation between *Hox13* and *Lin28* gene expression both *in vivo* and *in vitro* suggests that the progressive reduction in *Lin28*

expression observed in tail tissues of wild type embryos can likely result from the activation of *Hoxb13* and *Hoxc13* genes.

The specific regulatory network operating in tail tissues might account for one of the hallmarks of the secondary neural tube, namely its selective removal during morphogenesis of the final mature tail structures (Nievelstein et al., 1993). *Hox13* genes would play a critical role in this process. This idea is supported by the observation that the axial level where these *Hox* genes (most particularly *Hoxb13* and *Hoxc13*) become activated in mouse embryos fits well with the region of the neural tube fated to disappear. The caudally extended spinal cord observed in *Hoxb13* mutant embryos, which was proposed to derive from an incomplete elimination of the secondary neural tube (Economides et al., 2003), is also consistent with this hypothesis. A possible functional redundancy between *Hox13* genes might explain the relatively mild neural phenotype in the tail of the *Hoxb13* mutants, similarly to what has been observed for other *Hox* paralog groups (Mallo et al., 2010). *Hoxc13* could be among the best candidates for a possible redundant function given its expression pattern and the observation that the mutants have additional caudal vertebrae with lateral processes (Godwin and Capecchi, 1998), which could represent a caudal extension of the tail neural tube. Direct evaluation of this hypothesis will require generating the double *Hoxb13/Hoxc13* mutant, which has so far not been reported. However, *Gdf11* mutant embryos, in which these two genes are almost completely silent, fail to resorb the embryonic tail neural tube, producing mature structures in the newborn. Although it is not possible to be sure about the actual contribution of absent *Hox13* gene expression to this phenotype, considering the strong effect that premature *Hox13* expression has on the proliferation and apoptosis in *Sox2*-positive areas of the tail neural tube, it is likely that *Hox13* genes indeed play a substantial role in the tail spinal cord phenotype of *Gdf11* mutant embryos.

Hox13 gene activity in the tail neural tube might thus include two sequential processes. It would first limit spinal cord expansion in the areas fated to be resorbed. This effect might be mediated through the control of *Lin28* gene expression, as it is strongly reduced in the *Hoxb13* and *Hoxc13*-expressing areas of the tail neural tube and boosted in *Gdf11* mutant embryos, which fail to activate *Hoxb13/Hoxc13* expression. An inverse correlation between *Hox13* and

Lin28 gene expression was also evident in cultured tail bud cells, also fitting with their growth properties. Whether *Lin28* regulation by Hox13 proteins is direct or indirect remains to be determined.

Later in development, *Hox13* genes might activate apoptosis, eventually leading to tail neural tube elimination. This is supported by the reduced cell death observed in persistent areas of the tail spinal cord of *Hoxb13* mutant embryos (Economides et al., 2003). In addition, we observed an increase of apoptotic figures in the tail neural tube of *Cdx2-Hoxb13* embryos. This second *Hox13* activity might actually explain the absence of larger neural tubes in *Cdx2-Lin28* transgenics: as the *Cdx2* enhancer is active only in progenitor-containing areas, with very little extension into the neural tube, any extra spinal cord resulting from the activated progenitors would be subsequently eliminated by *Hox13* gene activity as part of the normal physiology of tail development.

Regulation of *Lin28* and *Hox13* expression in the tail

The observed expression dynamics of the *Lin28* genes indicates a change in their regulation coincident with the start of tail development. In particular, while their expression is not restricted to tail tissues, their transcripts only accumulate specifically in the tail region of *Gdf11* mutant embryos. The mechanism by which this regulation is carried out is not known but it is most likely related to the changes that the progenitors undergo during the trunk to tail transition. The expression pattern observed in the *Gdf11* embryos actually suggests that *Lin28* gene regulation undergoes a major change in their regulation when NMPs move from the epiblast to the tail bud. Gdf11 signaling might play a role in this process, as it is one of the key drivers of the trunk to tail transition [with partial redundancy of Gdf8 (McPherron et al., 2009)]. However, regardless of the role Gdf11 might play in this process, it is most likely permissive, facilitating the necessary changes in the cell biology of the progenitor cells intrinsic to their relocation into the tail bud.

Gdf11 signaling might play a more direct role in the control of *Hox13* gene expression. Indeed, this signaling pathway has already been shown to play a key role in the activation of posterior *Hox* genes (10 to 13 paralogs) (Deschamps and Duboule, 2017; Gaunt et al., 2013; Jurberg et al., 2013; Mallo, 2018).

Lin28 activity in the tail bud progenitors

It has been recently reported that aerobic glycolysis is essential for the activity of tail bud progenitors (Oginuma et al., 2017). Interestingly, *Lin28* genes have been implicated in the regulation of glucose metabolism, an activity that has been suggested to be mechanistically linked to their capacity to stimulate cancer progression by triggering the Warburg effect (Zhu et al., 2011). It is thus possible that promotion of aerobic glycolysis could be part of the mechanism by which *Lin28* genes control expansion and/or maintenance of tail bud axial progenitors. In this regard, several genes associated with this metabolic pathway seem to exhibit higher expression scores in *Gdf11* mutants than in wild type controls in our tail bud RNA-seq datasets (Fig. S3C). Although this is clearly too preliminary, it still suggests that the *Lin28*/metabolic connection in tail bud progenitors might be worth exploring in further detail. Similarly, it will be important to understand whether Lin28 activity in tail bud axial progenitors is functionally linked to the *let-7* miRNA family, as it does in other biological contexts (Zhu et al., 2011), or it follows alternative pathways.

***The Gdf11Lin28/Hox13* network and tail size variability.**

Quantitative differences within the *Gdf11/Lin28/Hox13* network might account for the tail size variability observed among vertebrate species. In particular, the timing of *Hox13* gene activation relative to the onset of the *Lin28*-dependent NMP phase might play a relevant role in this process. Another important parameter in tail length determination might result from the relative intensity of each of the components' activity in this network, either as a result of their expression level or of the intrinsic functional strength of their gene products. Experimental data gives support to this hypothesis. For instance, anticipating *Hox13* expression in transgenic mouse embryos shortened considerably their tail. Conversely, reducing the *Hox13* dosage or increasing the *Lin28* expression levels in the tail significantly extended its length. Therefore, it will be important to test these parameters in embryos of vertebrate species with different tail sizes. Interestingly, in chicken – a shot tailed species -, *Hoxb13* expression encompasses most of the tail bud (Denans et al., 2015). Full understanding of the mechanisms regulating tail size will require not only

identifying how Gdf11 signaling controls *Lin28* and *Hox13* activities, but also the pathways downstream of *Lin28* and *Hox13* genes.

AUTHOR CONTRIBUTION

Conceptualization: R.A. and M.M.; Methodology: R.A., L.M. and M.M.; Investigation: R.A., L.M., A.N., A.D.J. and M.M.; Writing-Original Draft: R.A. and M.M.; Writing-Review & Editing: R.A., M.M., D.D.; Resources: B.M. and D.D.; Funding Acquisition: M.M. and D.D.; Supervision: M.M.

ACKNOWLDEDGEMENTS

We would like to thank Alexandra McPherron and Se-Jin Lee for providing the *Gdf11* mutant strain, Jacqueline Deschamps for the *Cdx2* enhancer, Achim Gossler, and Michael Wegner for *in situ* probes, Daniel Sobral for the help with the analysis of the RNA-seq data, the IGC animal house for their help with animal housing, and members of the Mallo lab for useful comments during the course of this project. This work has been supported by grants PTDC/BEX-BID/0899/2014 (FCT, Portugal) and SCML-MC-60-2014 (from Santa Casa da Misericordia de Lisboa, Portugal) to M.M. and from the university of Geneva and the Swiss National Research Fund (No. 310030B-138662) to D.D.

DECLARATION OF INTERESTS

The authors declare no competing interests.

REFERENCES

Abu-Abed, S., Dollé, P., Metzger, D., Beckett, B., Chambon, P., Petkovich, M., 2001. The retinoic acid-metabolizing enzyme, CYP26A1, is essential for normal hindbrain patterning, vertebral identity, and development of posterior structures. Genes Dev. 15, 226–240. doi:10.1101/gad.855001

Aires, R., Dias, A., Mallo, M., 2018. Deconstructing the molecular mechanisms shaping the vertebrate body plan. Curr. Opin. Cell Biol. 55, 81–86. doi:10.1016/j.ceb.2018.05.009

Aires, R., Jurberg, A.D., Leal, F., Nóvoa, A., Cohn, M.J., Mallo, M., 2016. Oct4 Is a Key Regulator of Vertebrate Trunk Length Diversity. Dev. Cell 38, 262–274. doi:10.1016/j.devcel.2016.06.021

Andersson, O., Reissmann, E., Ibáñez, C.F., 2006. Growth differentiation factor 11 signals through the transforming growth factor-beta receptor ALK5 to regionalize the anterior-posterior axis. EMBO Rep. 7, 831–7. doi:10.1038/sj.embor.7400752

Benahmed, F., Gross, I., Gaunt, S.J., Beck, F., Jehan, F., Domon–Dell, C.,

Martin, E., Kedinger, M., Freund, J., Duluc, I., 2008. Multiple Regulatory Regions Control the Complex Expression Pattern of the Mouse Cdx2 Homeobox Gene. Gastroenterology 135, 1238–1247.e3. doi:10.1053/j.gastro.2008.06.045
Boulet, A.M., Capecchi, M.R., 2012. Signaling by FGF4 and FGF8 is required for axial elongation of the mouse embryo. Dev. Biol. 371, 235–245. doi:10.1016/j.ydbio.2012.08.017
Cambray, N., Wilson, V., 2007. Two distinct sources for a population of maturing axial progenitors. Development 134, 2829–2840. doi:10.1242/dev.02877
Cambray, N., Wilson, V., 2002. Axial progenitors with extensive potency are localised to the mouse chordoneural hinge. Development 129, 4855–4866. doi:10.1016/s0925-4773(98)00015-x
Casaca, A., Nóvoa, A., Mallo, M., 2016. Hoxb6 can interfere with somitogenesis in the posterior embryo through a mechanism independent of its rib-promoting activity. Development 143, 437–448. doi:10.1242/dev.133074
Danielian, P.S., Muccino, D., Rowitch, D.H., Michael, S.K., McMahon, A.P., 1998. Modification of gene activity in mouse embryos in utero by a tamoxifen-inducible form of Cre recombinase. Curr. Biol. 8, 1323-S2. doi:10.1016/S0960-9822(07)00562-3
Denans, N., Iimura, T., Pourquié, O., 2015. Hox genes control vertebrate body elongation by collinear Wnt repression. Elife 4, e04379. doi:10.7554/eLife.04379
Deschamps, J., Duboule, D., 2017. Embryonic timing, axial stem cells, chromatin dynamics, and the Hox clock. Genes Dev. 31, 1406–1416. doi:10.1101/gad.303123.117
DeVeale, B., Brokhman, I., Mohseni, P., Babak, T., Yoon, C., Lin, A., Onishi, K., Tomilin, A., Pevny, L., Zandstra, P.W., Nagy, A., van der Kooy, D., 2013. Oct4 Is Required ~E7.5 for Proliferation in the Primitive Streak. PLoS Genet. 9, e1003957. doi:10.1371/journal.pgen.1003957
Economides, K.D., Zeltser, L., Capecchi, M.R., 2003. Hoxb13 mutations cause overgrowth of caudal spinal cordand tail vertebrae. Dev. Biol. 256, 317–330. doi:10.1016/S0012-1606(02)00137-9
Eden, E., Lipson, D., Yogev, S., Yakhini, Z., 2007. Discovering motifs in ranked lists of DNA sequences. PLoS Comput. Biol. 3, e39. doi:10.1371/journal.pcbi.0030039
Eden, E., Navon, R., Steinfeld, I., Lipson, D., Yakhini, Z., 2009. GOrilla: A tool for discovery and visualization of enriched GO terms in ranked gene lists. BMC Bioinformatics 10, 48. doi:10.1186/1471-2105-10-48
Garriock, R.J., Chalamalasetty, R.B., Kennedy, M.W., Canizales, L.C., Lewandoski, M., Yamaguchi, T.P., 2015. Lineage tracing of neuromesodermal progenitors reveals novel Wnt-dependent roles in trunk progenitor cell maintenance and differentiation. Development 142, 1628–1638. doi:10.1242/dev.111922
Gaunt, S.J., George, M., Paul, Y.L., 2013. Direct activation of a mouse Hoxd11 axial expression enhancer by Gdf11/Smad signalling. Dev. Biol. 383, 52–60. doi:10.1016/j.ydbio.2013.08.025
Godwin, A.R., Capecchi, M.R., 1998. Hoxc13 mutant mice lack external hair. Genes Dev. 12, 11–20. doi:10.1101/gad.12.1.11
Gokoffski, K.K., Wu, H.-H., Beites, C.L., Kim, J., Kim, E.J., Matzuk, M.M.,

Johnson, J.E., Lander, A.D., Calof, A.L., 2011. Activin and GDF11 collaborate in feedback control of neuroepithelial stem cell proliferation and fate. Development 138, 4131–4142. doi:10.1242/dev.065870
Gouti, M., Tsakiridis, A., Wymeersch, F.J., Huang, Y., Kleinjung, J., Wilson, V., Briscoe, J., 2014. In vitro generation of neuromesodermal progenitors reveals distinct roles for wnt signalling in the specification of spinal cord and paraxial mesoderm identity. PLoS Biol. 12, e1001937. doi:10.1371/journal.pbio.1001937
Greco, T.L., Takada, S., Newhouse, M.M., McMahon, J.A., McMahon, A.P., Camper, S.A., 1996. Analysis of the vestigial tail mutation demonstrates that Wnt-3a gene dosage regulates mouse axial development. Genes Dev. 10, 313–324. doi:10.1101/gad.10.3.313
Henrique, D., Abranches, E., Verrier, L., Storey, K.G., 2015. Neuromesodermal progenitors and the making of the spinal cord. Development 142, 2864–2875. doi:10.1242/dev.119768
Herrmann, B.G., Labeit, S., Poustka, A., King, T.R., Lehrach, H., 1990. Cloning of the T gene required in mesoderm formation in the mouse. Nature 343, 617–622.
Ho, H.-Y.H., Susman, M.W., Bikoff, J.B., Ryu, Y.K., Jonas, A.M., Hu, L., Kuruvilla, R., Greenberg, M.E., 2012. Wnt5a-Ror-Dishevelled signaling constitutes a core developmental pathway that controls tissue morphogenesis. Proc. Natl. Acad. Sci. 109, 4044–4051. doi:10.1073/pnas.1200421109
Hogan, B., Beddington, R., Constantini, F., Lacy, E., 1994. Manipulating the mouse embryo: a laboratory manual, 2nd ed. Cold Spring Harbour Laboratory Press.
Javali, A., Misra, A., Leonavicius, K., Acharya, D., Vyas, B., Sambasivan, R., 2017. Co-expression of Tbx6 and Sox2 identifies a novel transient neuromesoderm progenitor cell state. Development 144, 4522–4529. doi:10.1242/dev.153262
Jurberg, A.D., Aires, R., Nóvoa, A., Rowland, J.E., Mallo, M., 2014. Compartment-dependent activities of Wnt3a/β-catenin signaling during vertebrate axial extension. Dev. Biol. 394, 253–263. doi:10.1016/j.ydbio.2014.08.012
Jurberg, A.D., Aires, R., Varela-Lasheras, I., Nóvoa, A., Mallo, M., 2013. Switching axial progenitors from producing trunk to tail tissues in vertebrate embryos. Dev. Cell 25, 451–462. doi:10.1016/j.devcel.2013.05.009
Langmead, B., Salzberg, S.L., 2012. Fast gapped-read alignment with Bowtie 2. Nat. Methods 9, 357–359. doi:10.1038/nmeth.1923
Lauschke, V.M., Tsiairis, C.D., François, P., Aulehla, A., 2013. Scaling of embryonic patterning based on phase-gradient encoding. Nature 493, 101–5. doi:10.1038/nature11804
Lee, Y.J., McPherron, A., Choe, S., Sakai, Y., Chandraratna, R.A., Lee, S.J., Oh, S.P., 2010. Growth differentiation factor 11 signaling controls retinoic acid activity for axial vertebral development. Dev. Biol. 347, 195–203. doi:10.1016/j.ydbio.2010.08.022
Mallo, M., 2018. Reassessing the Role of Hox Genes during Vertebrate Development and Evolution. Trends Genet. 34, 209–217. doi:10.1016/j.tig.2017.11.007
Mallo, M., Wellik, D.M., Deschamps, J., 2010. Hox genes and regional

patterning of the vertebrate body plan. Dev. Biol. 344, 7–15. doi:10.1016/j.ydbio.2010.04.024
Martin, B.L., Kimelman, D., 2008. Regulation of Canonical Wnt Signaling by Brachyury Is Essential for Posterior Mesoderm Formation. Dev. Cell 15, 121–133. doi:10.1016/j.devcel.2008.04.013
McPherron, A.C., Huynh, T. V, Lee, S.-J., 2009. Redundancy of myostatin and growth/differentiation factor 11 function. BMC Dev. Biol. 9, 24. doi:10.1186/1471-213X-9-24
McPherron, A.C., Lawle, A.M., Lee, S.-J., 1999. Regulation of anterior/posterior patterning of the axial skeleton by growth/differentiation factor 11. Nat. Genet. 22, 260–264. doi:10.1038/10320
Naiche, L. a, Holder, N., Lewandoski, M., 2011. FGF4 and FGF8 comprise the wavefront activity that controls somitogenesis. Proc. Natl. Acad. Sci. U. S. A. 108, 4018–4023. doi:10.1073/pnas.1007417108
Nievelstein, R.A., Hartwig, N.G., Vermeij-Keers, C., Valk, J., 1993. Embryonic development of the mammalian caudal neural tube. Teratology 48, 21–31.
Oginuma, M., Moncuquet, P., Xiong, F., Karoly, E., Guevorkian, K., Pourquie, O., 2017. A Gradient of Glycolytic Activity Coordinates FGF and Wnt Signaling during Elongation of the Body Axis in Amniote Embryos. Dev. Cell 40, 342–353. doi:10.1016/j.devcel.2017.02.001
Osorno, R., Tsakiridis, A., Wong, F., Cambray, N., Economou, C., Wilkie, R., Blin, G., Scotting, P.J., Chambers, I., Wilson, V., 2012. The developmental dismantling of pluripotency is reversed by ectopic Oct4 expression. TL - 139. Development 139, 2288–2298. doi:10.1242/dev.078071
Psychoyos, D., Stern, C.D., 1996. Fates and migratory routes of primitive streak cells in the chick embryo. Development 122, 1523–1534.
Sakai, Y., Meno, C., Fujii, H., Nishino, J., Shiratori, H., Saijoh, Y., Rossant, J., Hamada, H., 2001. The retinoic acid-inactivating enzyme CYP26 is essential for establishing an uneven distribution of retinoic acid along the anterio-posterior axis within the mouse embryo. Genes Dev. 15, 213–225. doi:10.1101/gad.851501
Savory, J.G.A., Mansfield, M., Rijli, F.M., Lohnes, D., 2011. Cdx mediates neural tube closure through transcriptional regulation of the planar cell polarity gene *Ptk7*. Development 138, 1361–1370. doi:10.1242/dev.056622
Schoenwolf, G.C., Smith, J.L., 1990. Mechanisms of neurulation: traditional viewpoint and recent advances. Development 109, 243–270.
Shi, Y., Liu, J.-P., 2011. Gdf11 facilitates temporal progression of neurogenesis in the developing spinal cord. J. Neurosci. 31, 883–893. doi:10.1523/JNEUROSCI.2394-10.2011
Shifley, E.T., VanHorn, K.M., Perez-Balaguer, A., Franklin, J.D., Weinstein, M., Cole, S.E., 2008. Oscillatory lunatic fringe activity is crucial for segmentation of the anterior but not posterior skeleton. Development 135, 899–908. doi:10.1242/dev.006742
Soriano, P., 1999. Generalized lacZ expression with the ROSA26 Cre reporter strain. Nat. Genet. 21, 70–71. doi:10.1038/5007
Southard-Smith, E.M., Kos, L., Pavan, W.J., 1998. Sox10 mutation disrupts neural crest development in Dom Hirschsprung mouse model. Nat. Genet. 18, 60–64. doi:10.1038/ng0598-51
Stern, C.D., Charité, J., Deschamps, J., Duboule, D., Durston, A.J., Kmita, M., Nicolas, J.F., Palmeirim, I., Smith, J.C., Wolpert, L., 2006. Head-tail

patterning of the vertebrate embryo: One, two or many unresolved problems? Int. J. Dev. Biol. 50, 3–15. doi:10.1387/ijdb.052095cs
Steventon, B., Martinez Arias, A., 2017. Evo-engineering and the Cellular and Molecular Origins of the Vertebrate Spinal Cord. Dev. Biol. 432, 3–13. doi:10.1101/068882
Suemori, H., Noguchi, S., 2000. Hox C Cluster Genes Are Dispensable for Overall Body Plan of Mouse Embryonic Development. Dev. Biol. 220, 333–342. doi:10.1006/dbio.2000.9651
Takada, S., Stark, K.L., Shea, M.J., Vassileva, G., McMahon, J.A., McMahon, A.P., 1994. Wnt-3a regulates somite and tailbud formation in the mouse embryo. Genes Dev. 8, 174–189. doi:10.1101/gad.8.2.174
Takemoto, T., Uchikawa, M., Yoshida, M., Bell, D.M., Lovell-Badge, R., Papaioannou, V.E., Kondoh, H., 2011. Tbx6-dependent Sox2 regulation determines neural or mesodermal fate in axial stem cells. Nature 470, 394–398. doi:10.1038/nature09729
Tesar, P.J., Chenoweth, J.G., Brook, F. a, Davies, T.J., Evans, E.P., Mack, D.L., Gardner, R.L., McKay, R.D., 2007. New cell lines from mouse epiblast share defining features with human embryonic stem cells. Nature 448, 196–199. doi:10.1038/nature05972
Trapnell, C., Hendrickson, D.G., Sauvageau, M., Goff, L., Rinn, J.L., Pachter, L., 2013. Differential analysis of gene regulation at transcript resolution with RNA-seq. Nat. Biotechnol. 31, 46–53. doi:10.1038/nbt.2450
Tsakiridis, A., Huang, Y., Blin, G., Skylaki, S., Wymeersch, F., Osorno, R.R., Economou, C., Karagianni, E., Zhao, S., Lowell, S., Wilson, V., 2014. Distinct Wnt-driven primitive streak-like populations reflect in vivo lineage precursors. Development 141, 1209–1221. doi:10.1242/dev.101014
Tzouanacou, E., Wegener, A., Wymeersch, F.J., Wilson, V., Nicolas, J.F., 2009. Redefining the Progression of Lineage Segregations during Mammalian Embryogenesis by Clonal Analysis. Dev. Cell 17, 365–376. doi:10.1016/j.devcel.2009.08.002
Viswanathan, S.R., Daley, G.Q., 2010. Lin28: A MicroRNA Regulator with a Macro Role. Cell 140, 445–449. doi:10.1016/j.cell.2010.02.007
Williams, D.R., Shifley, E.T., Lather, J.D., Cole, S.E., 2014. Posterior skeletal development and the segmentation clock period are sensitive to Lfng dosage during somitogenesis. Dev. Biol. 388, 159–169. doi:10.1016/j.ydbio.2014.02.006
Wilson, V., Beddington, R.S.P., 1996. Cell fate and morphogenetic movement in the late mouse primitive streak. Mech. Dev. 55, 79–89. doi:10.1016/0925-4773(95)00493-9
Wilson, V., Olivera-Martínez, I., Storey, K.G., 2009. Stem cells, signals and vertebrate body axis extension. Development 136, 1591–1604. doi:10.1242/dev.039172
Wymeersch, F.J., Huang, Y., Blin, G., Cambray, N., Wilkie, R., Wong, F.C.K., Wilson, V., 2016. Position-dependent plasticity of distinct progenitor types in the primitive streak. Elife 5, e10042. doi:10.7554/eLife.10042
Yamaguchi, T.P., Bradley, a, McMahon, a P., Jones, S., 1999. A Wnt5a pathway underlies outgrowth of multiple structures in the vertebrate embryo. Development 126, 1211–1223.
Yang, M., Yang, S.-L., Herrlinger, S., Liang, C., Dzieciatkowska, M., Hansen, K.C., Desai, R., Nagy, A., Niswander, L., Moss, E.G., Chen, J.-F., 2015.

Lin28 promotes the proliferative capacity of neural progenitor cells in brain development. Development 142, 1616–1627. doi:10.1242/dev.120543
Young, T., Rowland, J.E., van de Ven, C., Bialecka, M., Novoa, A., Carapuco, M., van Nes, J., de Graaff, W., Duluc, I., Freund, J.N., Beck, F., Mallo, M., Deschamps, J., 2009. Cdx and Hox Genes Differentially Regulate Posterior Axial Growth in Mammalian Embryos. Dev. Cell 17, 516–526. doi:10.1016/j.devcel.2009.08.010
Zhu, H., Ng, S.C., Segr, A. V., Shinoda, G., Shah, S.P., Einhorn, W.S., Takeuchi, A., Engreitz, J.M., Hagan, J.P., Kharas, M.G., Urbach, A., Thornton, J.E., Triboulet, R., Gregory, R.I., Altshuler, D., Daley, G.Q., 2011. The Lin28/let-7 axis regulates glucose metabolism. Cell 147, 81–94. doi:10.1016/j.cell.2011.08.033

STAR METHODS

CONTACT FOR REAGENT AND RESOURCE SHARING

Further information and requests for resources and reagents should be directed to and will be fulfilled by the Lead Contact, (mallo@igc.gulbenkian.pt). There are no specific restrictions for the use of materials within this manuscript.

EXPERIMENTAL MODEL AND SUBJECT DETAILS

Gdf11 mutant embryos were produced from intercrosses between *Gdf11*$^{+/-}$ mice (McPherron et al., 1999) (MGI Cat# 3589479, RRID:MGI:3589479). The *HoxCΔ* mutants (MGI:3640654) have been previously described (Suemori and Noguchi, 2000). For lineage tracing experiments, *Gdf11* heterozygous males containing the *Cdx2-Cre*^{ERT} transgene (*Gdf11*$^{+/-}$*::Cdx2-Cre*$^{ERT+/+}$) (Jurberg et al., 2013) were crossed with *Gdf11* heterozygous females that additionally carried a knock-in Cre-inducible *LacZ* allele in the ROSA26 locus [FVB.129S4(B6)-Gt(ROSA)26Sor$^{<tm1Sor>}$/J, stock No: 09427, Jackson] (Soriano, 1999) (*Gdf11*$^{+/-}$*::ROSA26r-β-gal*$^{+/0}$ mice), to generate *Gdf11*$^{-/-}$*::Cdx2- Cre*$^{ERT+/0}$*::ROSA26r-β-gal*$^{+/0}$ embryos. To generate the transgenic embryos and fetuses expressing the *Hoxb13*, *Hoxc13*, *Lin28a* and *Lin28b* genes, constructs were prepared by cloning the relevant cDNAs under the control of the *Cdx2* enhancer (Benahmed et al., 2008) and the SV40 polyadenylation signal. The *Cdx2-HoxC13* transgenic construct has been previously described (Young et al., 2009). The DNA constructs were liberated from vector sequences, gel purified and used to produce transgenic embryos by pronuclear injection according to standard procedures (Hogan et al., 1994). All primers used to generate the cDNAs can be found in the Key Resource Table.

Genotyping

Pups and adult mice were genotyped from tail biopsies. Samples were incubated overnight at 55º C in PBND buffer (50 mM KCl, 10 mM Tris-HCl pH 8.3, 2.5 mM $MgCl_2$, 0.1 mg/ml gelatin, 0.45% Nonidet P40 (NP40), 0.45% Tween 20) containing 200 µg/ml proteinase K (Roche). Lysates were then heat-inactivated for 15 minutes at 95ºC before being used for the genotyping PCR reactions. Embryos and fetuses were genotyped by PCR using genomic DNA extracted from yolk sacs (embryos), and intestines or skin (fetuses). When yolk sacs were used, they were incubated overnight at 55º C in yolk sac lysis buffer (50 mM KCl, 10 mM Tris-HCl pH 8.3, 2 mM $MgCl_2$, 0.45% Tween-20, 0.45% NP40) containing 200 µg/ml of proteinase K. Lysates were heat-inactivated as above. When intestine or skin samples were used, they were incubated overnight at 50º C under agitation in Laird's buffer (100 mM Tris-HCl pH 8.5, 5 mM EDTA, 0.2% SDS, 200 mM NaCl) supplemented with 100 µg/ml of proteinase K. Genomic DNA was then precipitated with isopropanol (1:1 vol:vol) and transferred to TE buffer (1 mM EDTA, 10 mM Tris-HCl pH8.0). All genotyping PCR reactions were performed using 1.5 µl of the genomic DNA

solution. All primers used for genotyping are described in the Key Resource Table.

Ethics statement

Experiments involving animals carried out in the Oeiras laboratory followed the Portuguese (Portaria 1005/92) and European (Directive 2010/63/EU) legislations, concerning housing, husbandry, and welfare. The project was reviewed and approved by the Ethics Committee of “Instituto Gulbenkian de Ciência” and by the Portuguese National Entity, “Direcção Geral de Alimentação Veterinária” (license reference: 014308). Experiments involving animals carried out in the Geneva laboratory were performed in agreement with the Swiss law on animal protection (LPA), under license No GE 81/14 (to DD).

METHOD DETAIL

Skeletal analyses

Skeletal preparations were performed at E18.5 by alcian blue/alizarin red staining. Fetuses were obtained by caesarean section, skinned, eviscerated and fixed in 100% ethanol at room temperature for at least 12 hours. They were stained with alcian blue 8 GX (150 mg/l in 20% acetic acid, 80% ethanol) at room temperature for 12 hours and postfixed in 100% ethanol for 12 hours. Fetuses were cleared in 2% KOH for 8 hours at room temperature, stained with alizarin red S (50 mg/l in 2% KOH) for 2 hours and further cleared in 2% KOH for 10 to 16 hours at room temperature. The reaction was stopped with 25% glycerol and the stained carcasses stored in the same solution. Caudal vertebrae were counted in a minimum of 10 embryos for each condition and statistical significance was assessed using non-parametric one-way ANOVA with Dunn’s multiple comparison test (alpha=0.05).

Histological analyses

Embryos were collected by caesarean section, dissected in Dulbecco’s Phosphate Buffered Saline (PBS) (1.8 mM KH_2PO_4, 2.7 mM KCl, 10 mM Na_2HPO_4, 137 mM NaCl) and fixed in Bouin’s fixative (Sigma) for one overnight (E10.5) or two days (E18.5). They were then dehydrated thoroughly in ethanol 100%, washed extensively in toluol and embedded in paraffin. Embryos were sectioned at 10 µm with a microtome and stained with haematoxylin and eosin according to standard methods.

In situ hybridization

Whole mount *in situ* hybridization was performed using *in vitro* transcribed digoxigenin-labelled antisense RNA probes. Briefly, embryos were dissected out in PBS and fixed with 4% paraformaldehyde (Sigma) made in PBS (PFA) at 4ºC overnight. Embryos were washed in PBT (PBS containing 0.1% Tween-20), dehydrated with methanol and rehydrated with PBT. They were then treated with proteinase K (10 µg/ml in PBT) at room temperature for 9 minutes for

E10.5 embryos, 12 minutes for E11.5, 15 min for E12.5 embryos, and 16 min for E13.5 embryos. The reaction was stopped with glycine (2 mg/ml in PBT) and embryos were postfixed with 4% paraformaldehyde, 0.2% glutaraldehyde (Sigma). Hybridization was performed at 70ºC overnight in hybridization solution [50% formamide, 1.3 x SSC (3M NaCl, 300 mM sodium citrate, pH 5.5), 5 mM EDTA, 0.2 % Tween 20, 50 µg/ml yeast tRNA, 100 µg/ml heparin] containing the RNA probe, followed by three washes at 70ºC in hybridization solution without the RNA probe, tRNA and heparin. Embryos were then washed in TBST (25 mM Tris.HCl, pH 8.0, 140 mM NaCl, 2.7 mM KCl, 0.1% Tween 20), equilibrated with MABT (100 mM Maleic acid, 150 mM NaCl, 0.1 % Tween-20, pH 7.5), blocked with MABT/Block [MABT containing 1% blocking reagent (Roche #11096176001) and 10% sheep serum] for 2-3h and incubated with a 1:2000 dilution of alkaline phosphatase-conjugated anti-digoxigenin antibody (Roche Cat# 11093274910, RRID:AB_514497) in MABT/Block at 4ºC overnight. Embryos were washed extensively with MABT at room temperature for 24h, equilibrated in NTMT (100 mM Tris HCl, pH 9.5, 50 mM $MgCl_2$, 100 mM NaCl, 0.1% Tween-20) and developed at room temperature with NBT/BCIP (Roche #11681451001) diluted in NTMT, or with BM Purple (Roche #11442074001). Reactions were stopped with PBT, fixed with 4% PFA and stored in PBT.

Probes for *Mesogenin1*, *Hoxb13*, *Hoxc13*, *Lin28a* and *Lin28b* were prepared by amplifying cDNA fragments and cloning them into appropriate vectors for in vitro transcription. The sequences for all used primers can be found in the Key Resource Table.

Post-staining embryo sectioning

To section whole mount-stained embryos, these were included in gelatin/albumin [0.45 % gelatin, 270 g/l bovine serum albumin (Roche), 180 g/l sucrose in PBS, jellified with 1.75 % glutaraldehyde]. Sections were cut at 35 µm with a vibratome and mounted with an aqueous mounting solution (Aquatex, Merck). Vibratome sections were photographed and used for measuring the areas of the neural tube, mesoderm and ectopic epithelial pocket in wild type and *Gdf11*$^{-/-}$ embryonic tails using Fiji (Fiji, RRID: SCR_002285). Two sections per tail at the PSM level were used, for a minimum of 10 embryos per condition. Statistical significance was assessed using an unpaired t-test using the Holm-Sidak method (alpha=0.05).

Fluorescence activated cell sorting (FACS)

Embryos were dissected in PBS and tails were pooled in 10% donkey serum in PBS. Tail tips were centrifuged at room temperature for 5 minutes at 1000 rpm and incubated on ice for 5 minutes with accutase. Tails were then dissociated into a single cell suspension and washed twice with PBS/10% donkey serum (Biowest S2170-100). Cells from both wild type and *Gdf11* mutant tails were counted and equivalent numbers for each condition were blocked for 30 minutes in 100 µl of blocking solution (10% donkey serum/1:100 Fc block in

PBS). Cells were processed for staining using True-Nuclear™ Transcription Factor Buffer Set (Biolegend) according to the manufacturer's instructions. They were incubated for 1 hour with primary antibodies against Sox2 (Abcam Cat# ab92494, RRID:AB_10585428) and T (R and D Systems Cat# AF2085, RRID:AB_2200235), diluted 1:200 in Perm buffer, washed twice in the same buffer and incubated for another hour with donkey anti-rabbit A568 (Thermo Fisher Scientific Cat# A10042, RRID:AB_2534017) and donkey anti-goat A647 (Thermo Fisher Scientific Cat# A-21447, RRID:AB_2535864) secondary antibodies, diluted 1:1000 in perm buffer. After three washes in perm buffer, cells were ressuspended in 300 µl PBS. Data acquisition was performed in a LSR Fortessa X20 flow cytometer. Gene expression levels were assessed after removing debris on the basis of the forward scatter-area (FSC-A) and side scatter signals (SSC-A). Doublets were removed using the FSC-A and forward scatter-width (FSC-W) signals. Quadrants were defined according to levels of background fluorescence as given by unstained and secondary-only incubated cell controls. FACS data was analyzed using FlowJo X software. Quadrant averages were calculated using 8 independent experiments. Statistical significance was assessed using the non-parametric Mann-Whitney test.

Lineage tracing analyses

Cre-mediated recombination was induced at E7.5 by a single intraperitoneal injection of 200 µl of a 1 mg/ml solution of tamoxifen (Sigma) in corn oil (Sigma). Embryos were collected at E10.5 by caesarean section, dissected in PBS and processed for β-galactosidase staining. Briefly, embryos were fixed with 4% PFA for 30 minutes at room temperature. After 3 washes with washing solution (PBS containing 0.02% NP40, 0.02% Tween 20) embryos were incubated at 37ºC in X-gal staining solution [5 mM $K_3Fe(CN)_6$, 5 mM $K_4Fe(CN)_6 \cdot 3H_2O$, 2 mM $MgCl_2$, 0.02% NP40, 0.02% Tween 20, in PBS, including 0.4 mg/ml X-gal (Promega)] and the reaction was monitored regularly. After developing, embryos were extensively washed in washing solution, fixed overnight in 4%PFA and embedded in gelatin/albumin as described above and sectioned with a vibratome. β-gal$^+$ cells were counted in 4 (trunk) or 9 (tail) consecutive sections using Fiji. The average number of cells per section in each compartment (neural tube or mesoderm) was calculated. Three embryos from each condition were used for this analysis. Statistical significance was assessed through an unpaired t-test using the Holm-Sidak method (alpha=0.05).

Tail explant cultures and serial passaging experiments

Wild type and *Gdf11* mutant embryos were collected in PBS at E10.5, their tails dissected and cultured as previously described (Tesar et al., 2007). Briefly, tails were severed from the embryo at the level of the last somite and incubated for 5 minutes in 1x accutase at 4ºC (Sigma, A6964). Tail tips were then washed three times with "N2B27 medium", which was constituted by Dulbecco's Modified Eagle Medium F12 (Gibco) and Neurobasal medium (Gibco) (1:1),

supplemented with 0.1 mM 2-mercaptoethanol (Sigma), 2 mM L-glutamine (Gibco), 40 mg/ml BSA (Sigma), 1x N2 (Gibco) and 1x B27 (Gibco) (Gouti et al., 2014). The tissue was mechanically dissociated to obtain 10-100 cell clumps. These were plated onto 24-well plates coated with a 50 µg/µl fibronectin solution in PBS (Lauschke et al., 2013) with the previously described "N2B27 medium", now supplemented with 20 ng/ml bFGF (R&D Systems), 3 µM CHIR (Abcam) and with or without 10 µM Alk-receptor inhibitor SB431542 (Abcam). Cells were allowed to grow at 37ºC with 5% CO_2 and their medium was changed every other day.

Cells were passaged every three days. Cell passaging was performed by washing wells twice with PBS, followed by five-minute incubation with accutase at RT. Cell suspensions were transferred to N2B27 medium without growth factor supplementation, centrifuged for 5 minutes at 1000 rpm, ressuspended in 500 µl of N2B27 medium and counted. $2x10^4$ cells were passaged onto new fibronectin-coated wells in 24-well plates or wells containing fibronectin-coated coverslips for immunofluorescence. Cells were grown as described above. Growth was plotted as the cumulative Population Doubling Levels (PDL) of four independent experiments and was calculated according to the formula PD= $\log_2$ (N2/N1), in which N1 represents the number of seeded cells and N2 the total number of cells obtained at the time of passaging. Statistical significance of the PDL in each time point for the set of 4 experiments was assessed using a two-way ANOVA where $p<0.05$ was considered significant. Linear regression was performed to calculate PDL growth ratio and the proliferation time was calculated by finding the inverse of this ratio (PDT=1/PDL). The PDL growth ratios obtained by linear regression were the following (expressed as doublings/day): WT- 0.42; WT+SB – 1.16, Gdf11 – 0.83, Gdf11+SB – 1.36. Statistical significance for the slopes was assessed using a non-parametric one-way ANOVA with Dunn's multiple comparison test (alpha=0.05).

Imunofluorescence

Immunofluorescence was performed on cultured cell explants or cryostat sections of embryos. Coverslips with attached explant cells were washed twice in PBS, fixed in 4% PFA for 15 minutes at room temperature and rinsed three times in PBS. After permeabilization in PBS 0.3% Triton-X for 15 minutes, cells were blocked for 1 hour in blocking solution (PBS/10% serum). Primary antibodies were diluted in blocking solution and incubated overnight at 4ºC. After three washes with PBS, slides were incubated with secondary antibodies diluted 1:1000 in blocking solution for 3-4 hours at room temperature. After extensive washing with PBS, nuclei were counterstained with 4', 6-Diamidino-2-Phenylindole Dilactate (DAPI) (Thermo Fisher Scientific Cat# D3571, RRID: AB_2307445) (1:1000 in PBS) and mounted in glass slides.

For immunofluorescence staining of tail tissues, after an overnight fixation with 4% PFA, embryos were washed thoroughly in PBS and incubated overnight at 4ºC in 15% sucrose (Sigma) in PBS and equilibrated with 15%

sucrose/7% gelatin (Sigma) in PBS for 2-6 hours at 37ºC. They were then transferred to appropriate moulds and frozen in liquid nitrogen. 14 µm-thick sagittal sections were obtained using a cryostat and adjacent sections collected in duplicate slides. For immunofluorescence, tissues were de-gelatinized, permeabilized with 0.1% Triton-X in PBS for 15 minutes and extensively washed with PBS. Sections were blocked in a 3% donkey serum (Biowest S2170-100)/1% BSA (Roche #10735086001) solution in PBST for 1 hour at room temperature. Primary antibodies were diluted in blocking solution and incubated overnight at 4ºC. Secondary antibodies were diluted in 1:1000 in blocking buffer and incubated for 3-4h at room temperature. After washes in PBS, slides were stained with DAPI (1:1000 in PBS) for 5 minutes.

The following primary antibodies were used in these experiments: goat anti-Brachyury (R and D Systems Cat# AF2085, RRID:AB_2200235; 1:250), mouse anti-Hoxb13 (Santa Cruz Biotechnology Cat# sc-28333, RRID:AB_627744; 1:100), mouse anti-Hoxc13 (sc-514377, Santa Cruz Biotechnology; 1:100), mouse anti-Nestin (Abcam Cat# ab6142, RRID:AB_305313; 1:250), goat anti-Lin28a (R and D Systems Cat# AF3757, RRID:AB_2234537; 1:200), goat anti-Tbx6 (R and D Systems Cat# AF4744, RRID:AB_2200834; 1:100), rabbit anti-Sox2 (Abcam Cat# ab92494, RRID:AB_10585428; 1:250), rabbit anti-Tuj1 (Abcam Cat# ab18207, RRID:AB_444319, 1:250). The secondary antibodies were: donkey anti-mouse Alexa 488 (Abcam Cat# ab150105, RRID:AB_2732856), donkey anti-goat Alexa Fluor 488 (Thermo Fisher Scientific Cat# A-11055, RRID:AB_2534102), donkey anti-goat Alexa Fluor 647 (Thermo Fisher Scientific Cat# A-21447, RRID:AB_2535864), and Alexa fluor 568 donkey anti-rabbit (Thermo Fisher Scientific Cat# A10042, RRID:AB_2534017).

Slides and tissue sections were mounted using VectaShield® (Vector Laboratories Cat# H-1000, RRID:AB_2336789). Confocal Z-series stacks of immunostained material were acquired on a Leica SP5 confocal microscope (Leica SP5 live; Leica Microsystems) using a 20x objective. Images were processed using Fiji software (NIH). A minimum of 10 images (optical sections) were used for each maximum projection Z-stack.

Apoptosis and proliferation analysis

Cell apoptosis was assessed using *in situ* cell death detection kit, fluorescein (#11684795910, Roche). Briefly, cryosectioned tissue was de-gelatinized, permeabilized and blocked as previously described for immunofluorescence. Primary antibodies for phospho-Histone 3 (Millipore Cat# 06-570, RRID:AB_310177) and Sox2 (Santa Cruz Biotechnology Cat# sc-17320, RRID:AB_2286684) were incubated 1:200 overnight in blocking solution. After rinsing three times in PBS, slides were incubated with 0.1% Triton-X in 0.1% sodium citrate for 2 minutes on ice, washed again and incubated for 1 hour with 50µl of TUNEL reaction mixture prepared according to the manufacturer's instructions. Tissue sections were then incubated 3-4h in secondary antibodies

donkey anti-goat Alexa Fluor 647 (Thermo Fisher Scientific Cat# A-21447, RRID:AB_2535864) and donkey anti-rabbit Alexa fluor 568 (Thermo Fisher Scientific Cat# A10042, RRID:AB_2534017) diluted 1:1000 in blocking solution. After extensive washes in PBS, samples were incubated with DAPI (1:1000 in PBS), mounted in Vectashield and imaged. Two to 6 sections from tails of 3 embryos from each condition were used. pH3 positive cells in each compartment were counted using Fiji and statistical significance was assessed using unpaired t-test using the Holm-Sidak method (alpha=0.05).

RNAseq

Total RNA was isolated from at least 8 tail buds obtained from E10.5 wild type and *Gdf11* mutant embryos using the RNeasy mini kit (Qiagen), according the manufacture's recommendations. The RNA quantity and purity were measured with a Nanodrop ND-100 spectrophotometer (Thermo Scientific). RNA integrity number (RIN) was determined with the AATI Fragment Analyzer. RNA-seq libraries from two biological replicates from each condition were prepared using TrueSeq stranded mRNA sample Prep Kit and sequenced using Illumina Hiseq 2500 system, to obtain 50 base single-end reads at CRG Genomics Unit (Barcelona, Spain). At least, 25 M of SE reads were generated for each library in a sequencing lane. Read alignments were made using Tophat2 v2.0.9 (Kim et al. 2013) with Bowtie v2.1.0.0 (Langmead and Salzberg, 2012). Differential expression analysis between wild type and *Gdf11* mutant samples was performed using CuffDiff v2.1.1 (Trapnell et al., 2013). Genes with FDR<0.05 were considered to be differentially expressed.

Gene Ontology (GO) analysis (Eden et al., 2009, 2007) was used to identify enriched GO process terms using a list of the top 88 genes that exhibited a $\log_2$Foldchange > 2 and q value < 0.005 in *Gdf11*$^{-/-}$ comparing to the WT.

RT-qPCR

Total RNA was extracted from cultured cells using Tri Reagent (Sigma) according to the manufacture's protocol, and resuspended in water. The total RNA concentration was determined with a Nanodrop ND-100 spectrophotometer. 1 ug of RNA was reverse-transcribed into complementary DNA (cDNA) using a random hexamer mix (NZYTech) and following the protocol of the NZY Reverse Transcriptase enzyme (NZYTech). Real-time PCR was performed with iQ SYBR Green Supermix (Bio-rad) according to manufacturer's instructions and using CFX384 Real Time PCR Detection System (Bio-Rad). Primers are listed in the Key Resource Table. The expression levels were normalized to β-Actin and changes in fold expression were calculated using the $\Delta\Delta C_t$ method. Gene expression data was presented as the mean ± SD. Differences were considered significant at *p<0.05, ** p<0.01, and ***p<0.001. Statistical significance was assessed using the non-parametric Mann-Whitney test.

IMAGE PROCESSING AND ANALYSIS

All image processing, analysis and measurements were performed using Fiji (Fiji, RRID:SCR_002285). Data was analyzed and plotted using GraphPad Prism7 (Graphpad Prism, RRID:SCR_002798).

QUANTIFICATION AND STATISTICAL ANALYSIS

The quantitation and statistical analyses associated with the different experimental procedures included in this paper are described in the corresponding subsections of the Method Details. Tail length analysis and comparison between wild type and *Lin28* transgenics is described at the end of the *skeletal analysis* subsection. The method used to calculate the progenitor cell number in the tail buds by FACS is specified at the end of the *fluorescence activated cell sorting (FACS)* subsection. The analysis of labelled progenitor contribution to different areas of the trunk and tail tissues is described at the end of the *Lineage tracing analyses* subsection. Details on the in vitro growth properties of explanted tail bud cells can be found at the end of the *Tail explant cultures and serial passaging experiments* subsection. The methods used for transcript quantification and content comparison between wild type and Gdf11 mutant embryos by RNA-seq and qPCR are specified at the end of the subsections where the experimental details of these procedures are described.

DATA AVAILABILITY

The raw sequencing data of the RNA-seq experiments was deposited in the NCBI trace and Short-read Archive (SRA), accession number SRP167717 (https://www.ncbi.nlm.nih.gov/Traces/study/?acc=SRP167717&go=go).

FIGURES

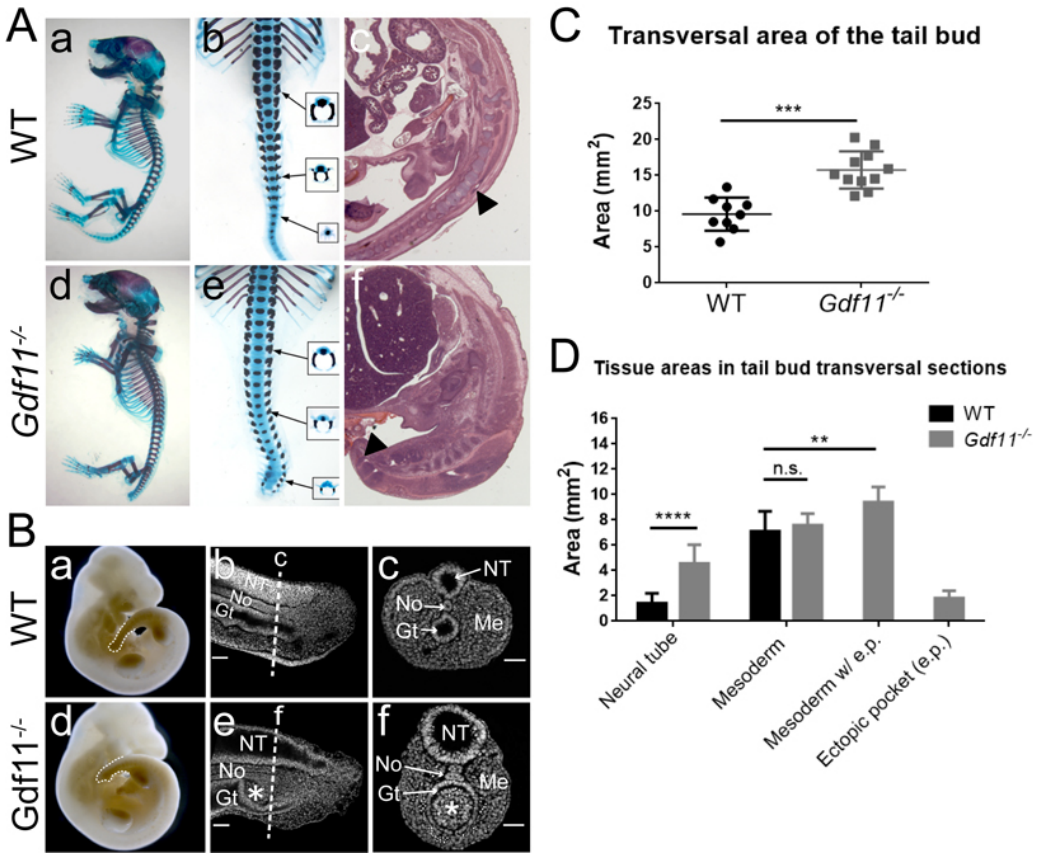

Figure 1. *Gdf11* mutant embryos exhibit tail malformations. A. Skeletal (a, b, d, e) and histological (c, f) analysis of E18.5 wild type (WT; a-c) and *Gdf11* mutant fetuses (*Gdf11*$^{-/-}$; d-f). Insets in b) and e) show dissected vertebrae at the indicated axial level. Black arrowheads indicate the caudal end of the neural tube. B. E10.5 wild type (a-c) and *Gdf11*$^{-/-}$ (d-f) embryos, as whole mount view (a, d) or in DAPI staining of sagittal (b, e) or transversal (c, f) sections through the tail. Dotted lines in a and d delimit and emphasize tail morphology. Dotted lines in b and e indicate the levels of the sections in c and f. NT, neural tube; No, notochord; Gt, gut; Me, mesoderm; the asterisk indicates the ectopic ventral epithelial pocket characteristic of *Gdf11* mutant tails. Scale bars: 100µm. C. Total area of transversal sections of wild type and *Gdf11*$^{-/-}$ tail buds at the level of the PSM (*** p<0.001). D. Total areas of the main tissue compartments in wild type and *Gdf11*$^{-/-}$ tail buds at the level of the PSM (**p<0.01, **** p<0.0001). Error bars indicate the standard deviation (SD).

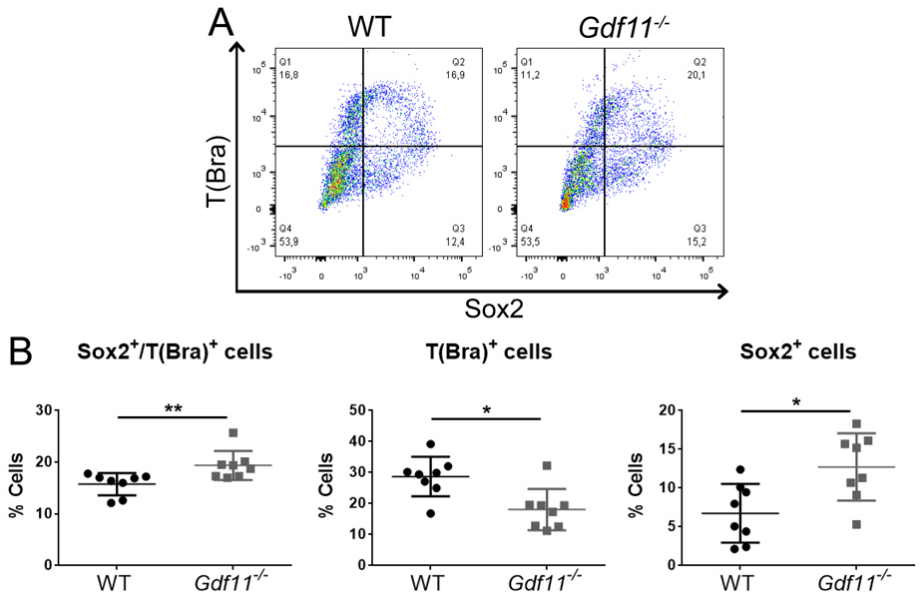

Figure 2. FACS analysis of Sox2 and T(Bra) expression in wild type and *Gdf11*$^{-/-}$ tail buds. A. Representative pseudo-color dot plots depicting the distribution of events and quadrants in wild type and *Gdf11*$^{-/-}$ tail buds. B. Proportion of cells co-expressing Sox2 and T (Bra) (quadrant 2 in the plots), or T (quadrant 1 in the plots) and Sox2 (quadrant 3 in the plots) alone in wild type and *Gdf11*$^{-/-}$ tail buds from 8 independent experiments (*p<0.05; **p<0.001). Error bars indicate the SD.

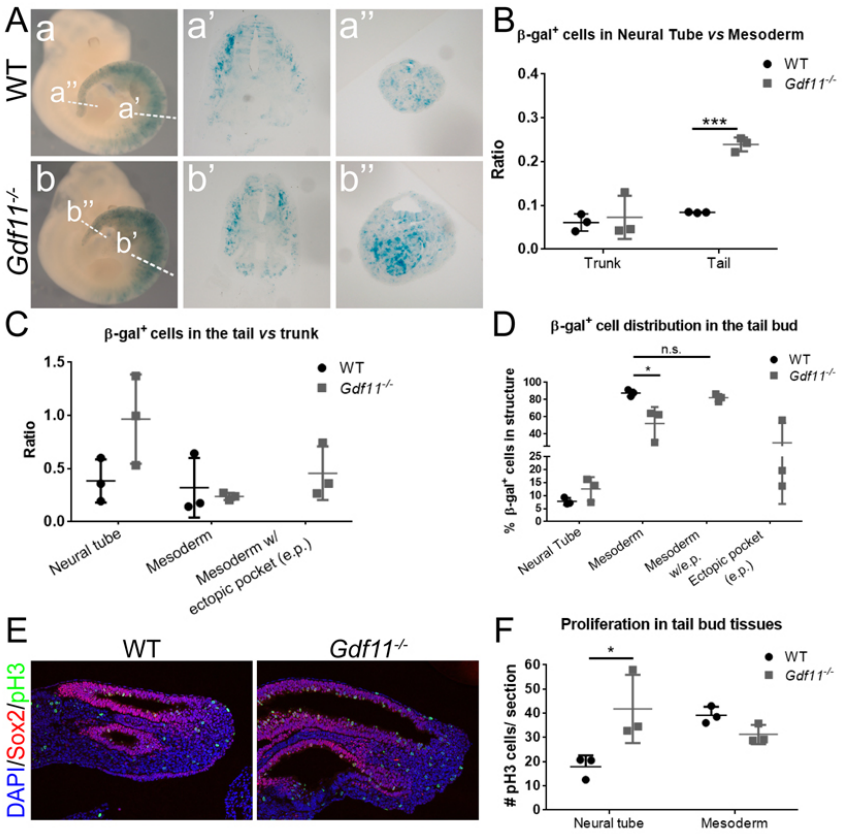

Figure 3. Lineage tracing analysis and proliferation in wild type and *Gdf11*$^{-/-}$ tail buds. A. β-gal staining of E10.5 wild type (a-a'') and *Gdf11*$^{-/-}$ (b-b'') embryos. a and b show whole mount views; a' and b' show sections at trunk levels; and a'' and b'' show sections at tail levels. Dotted lines in a and b indicate the levels of the sections. B. Differential contribution of β-gal^{+} cells to neural tube and mesoderm in the embryonic trunk and tail expressed as the ratio between stained cells in each compartment at the respective axial level (***p<0.001). C. Relative enrichment of β-gal^{+} cells in neural tube and mesoderm in the tail bud compared to the trunk. D. Distribution of β-gal^{+} cells in the different tissue compartments in the tail bud (*p<0.05). E. Immunofluorescence for Sox2 and pH3 in sagittal sections of wild type and *Gdf11*$^{-/-}$ tail buds. F. Quantification of cell proliferation in the neural tube and mesoderm of wild type and *Gdf11*$^{-/-}$ tail buds (*p<0.05). Each dot represents one independent experiment. Error bars indicate the SD from three independent experiments.

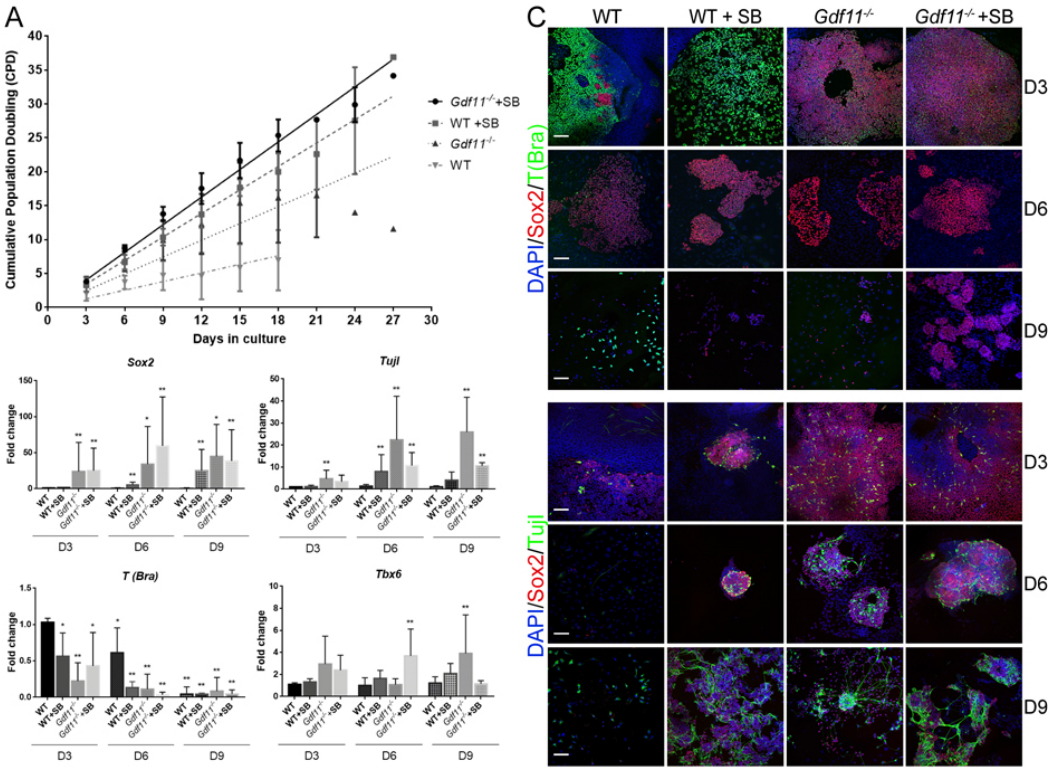

Figure 4. Culture of tail bud explants in the presence and absence of Gdf11 signalling. A. Growth as cumulative population doubling (CPD) and corresponding growth rates in cultures of E10.5 wild type and *Gdf11*$^{-/-}$ tail bud explants in the presence (+SB) or absence of the TGF-β inhibitor SB431542, subjected to serial passaging (every 3 days). Error bars indicate the SD of four independent experiments. B. Gene expression analysis by qRT-PCR for *Sox2*, *TujI, T(Bra)* and *Tbx6* in cultured tail bud explants 3 (D3), 6 (D6) and 9 (D9) days after plating. Expression in D3 wild type cells was used as the reference to represent relative expression levels obtained in each culture condition of the same time point (*p<0.05, **p<0.01). Error bars indicate the SD of six independent experiments. C. Immunofluorescence images of tail bud explants stained for Sox2 and T(Bra), or Sox2 and TujI at D3, D6 and D9 after seeding. Scale bars: 100μm.

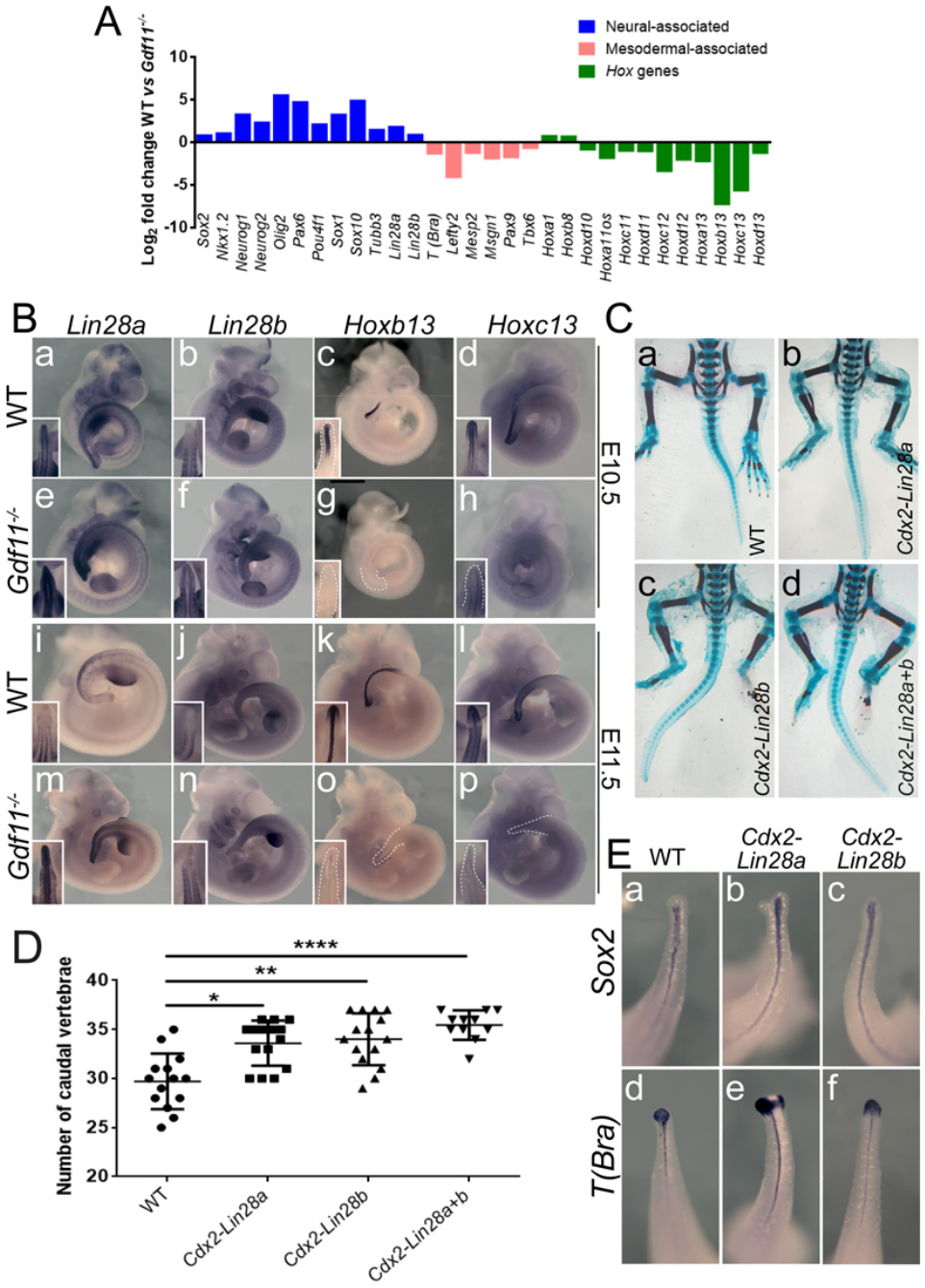

Figure 5. RNAseq analysis and validation in E10.5 and E11.5 wild type and *Gdf11*$^{-/-}$ embryonic tails. A. Fold change differences of representative neural (blue), mesodermal (pink), and *Hox* (green) genes between wild type and *Gdf11*$^{-/-}$ E 10.5 embryos. B. Whole mount *in situ* hybridization of wild type (a-d, i-l) and *Gdf11*$^{-/-}$ (e-h, m-p) embryos at E10.5 (a-h) or E11.5 (i-p) using probes for *Lin28a* (a, e, i, m), *Lin28b* (b, f, j, n), *Hoxb13* (c, g, k, o), and *Hoxc13* (d, h, l, p). Insets show dorsal views of the tail bud. Tail shapes are delimited by dotted lines. C. Skeletal preparations of tails from E18.5 wild type (a), *Cdx2-Lin28a* (b), *Cdx2-Lin28b* (c), and compound *Cdx2-Lin28a* + *Cdx2-Lin28b* (*Cdx2-Lin28a+b*) (d) fetuses. D. Number of caudal vertebrae in wild type, *Cdx2-Lin28a*, *Cdx2-Lin28b*, and *Cdx2-Lin28a+b* transgenic fetuses (*p<0.05, **p<0.01, ****p<0.0001). Each dot represents an individual specimen. Error bars indicate the SD. E. Dorsal view of whole mount *in situ* hybridization of E13.5 tails from wild type (a, d), *Cdx2-Lin28a* (b, e), and *Cdx2-Lin28b* (c, f) embryos using probes for *Sox2* (a-c) and *T(Bra)* (d-f).

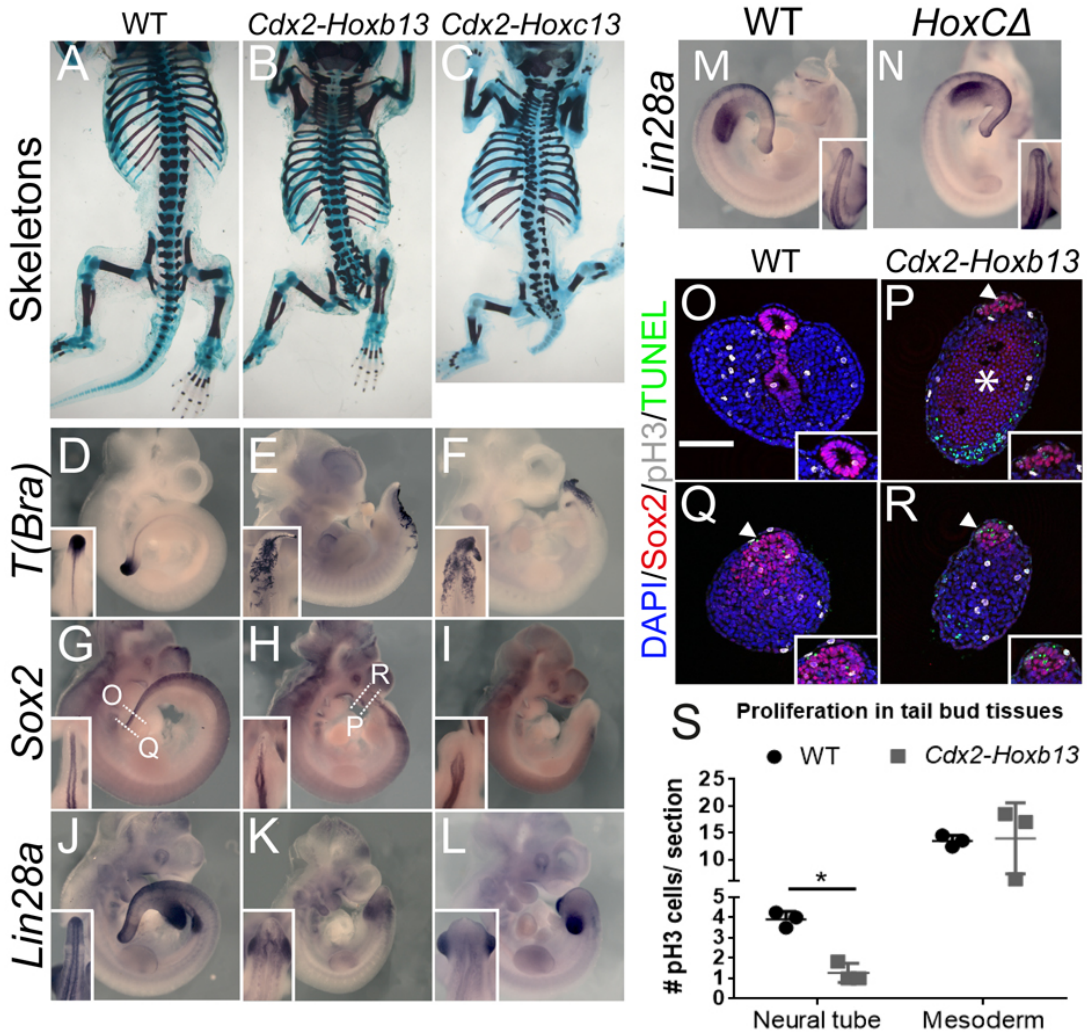

Figure 6. *Hoxb13* and *Hoxc13* overexpression specifically affects tail growth. A-C. Skeletal preparations of E18.5 wild type (A), *Cdx2-Hoxb13* (B) and *Cdx2-Hoxc13* (C) fetuses. D-L. Whole mount *in situ* hybridization of E10.5 wild type (D, G, J), *Cdx2-Hoxb13* (E, H, K), and *Cdx2-Hoxc13* (F, I, L) embryos with probes for *T(Bra)* (D-F), *Sox2* (G-I) and *Lin28a* (J-L). Insets show dorsal views of the tail. Dotted lines indicate the level of the sections displayed in O-R. M and N. Whole mount *in situ* hybridization on E10.5 wild type (M) or *HoxCΔ* (N) embryos with a probe for *Lin28a*. Insets show a dorsal view of the tail. O-R. Analysis of proliferation (pH3) and apoptosis (TUNEL) in transversal tail sections of E10.5 wild type (O, Q) and *Cdx2-Hoxb13* (P, R) embryos. Insets depict a close-up of the neural tube (stained with Sox2). White arrowheads indicate cell death in the neural tube. The asterisk indicates blood accumulation. Scale bar: 100µm. S. Quantification of cell proliferation in the neural tube and mesoderm of wild type and *Cdx2-Hoxb13* tails (*p<0.05). Error bars indicate the SD from three independent experiments.

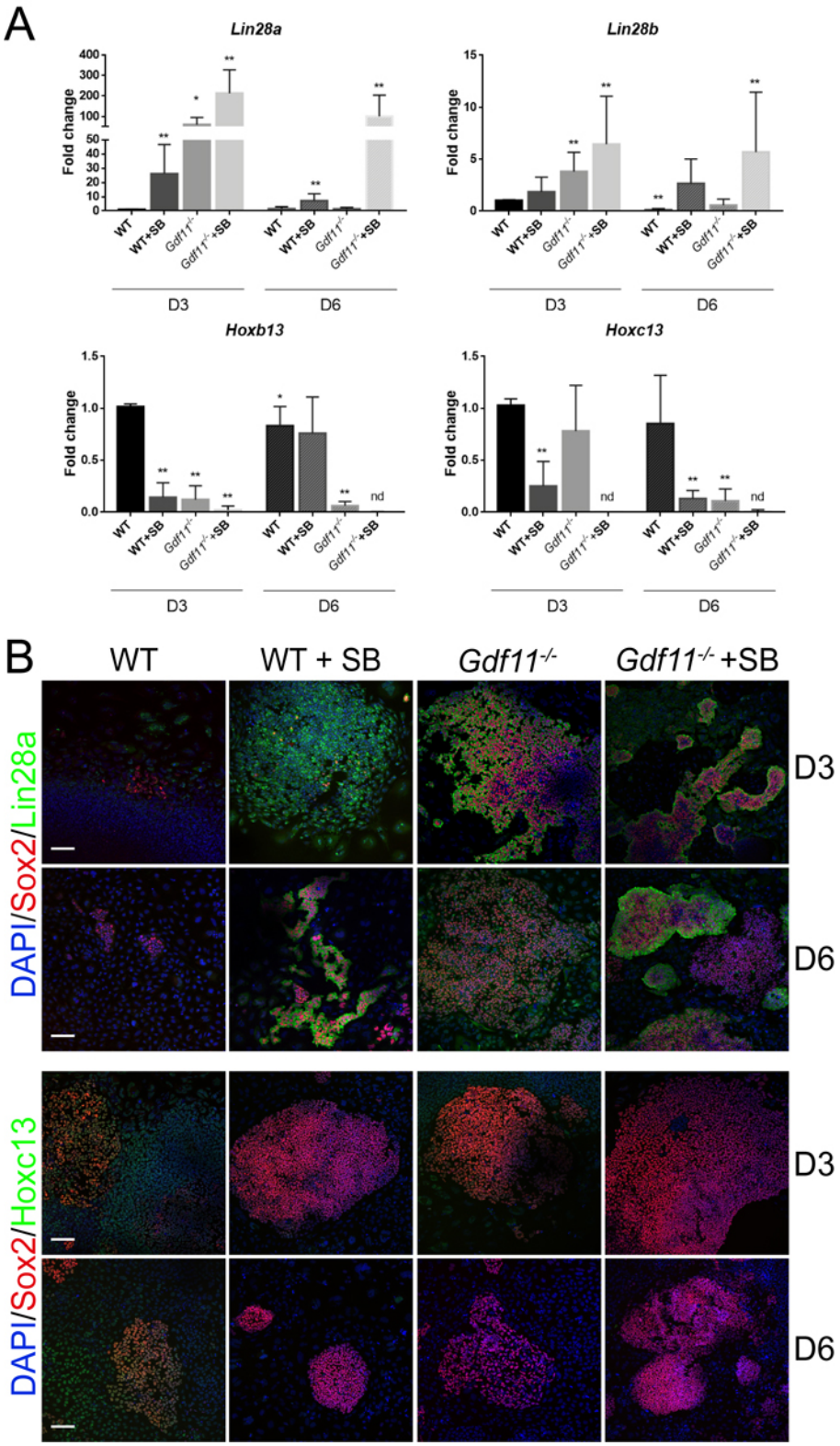

Figure 7. Gdf11 signalling controls expression of *Lin28* genes, *Hoxb13* and *Hoxc13* in tail bud explant cultures. A. qRT-qPCR analysis of *Lin28a*, *Lin28b*, *Hoxb13*, and *Hoxc13* expression in explant cultures at D3 and D6. Expression in D3 wild type cells was used as the reference to represent relative expression levels obtained in each culture condition of the same time point (*p<0.05, **p<0.01). Error bars indicate the SD of six independent experiments. B. Immunofluorescence images of tail bud explants stained for Sox2 and Lin28a, or Sox2 and Hoxc13 at day 3 (D3) or day 6 (D6) after seeding. Scale bars: 100µm.

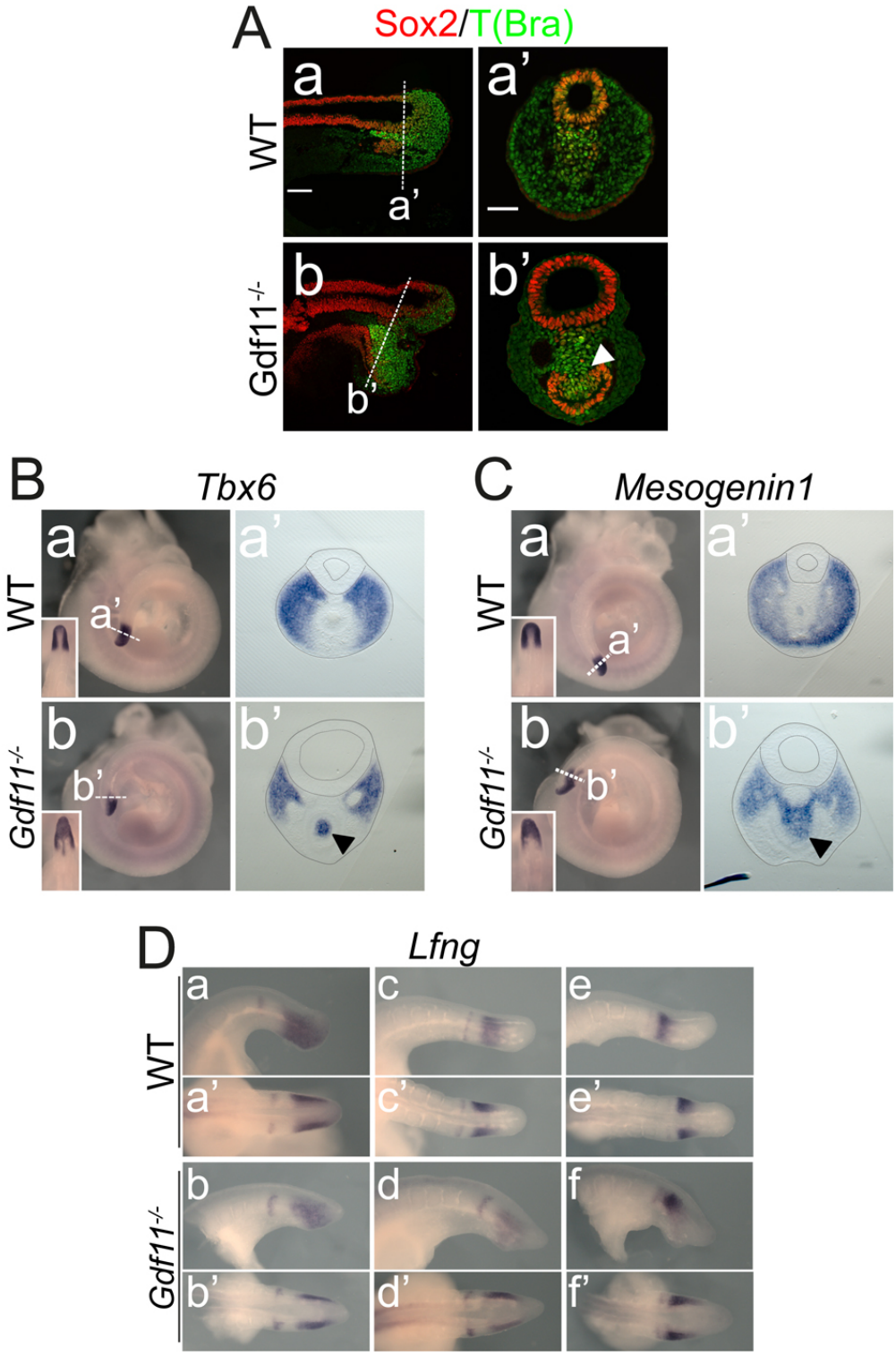

Figure S1. Related to Figure 3. Gene expression in E10.5 wild type and *Gdf11*$^{-/-}$ embryonic tails. A. Immunofluorescence images of sagittal (a, b) and transversal (a', b') sections of wild type (a, a') and *Gdf11*$^{-/-}$ (b, b') tail buds stained for Sox2 and T(Bra). Dotted lines indicate the level of transversal sections in a' and b'. White arrowhead indicates the ectopic epithelial pocket in *Gdf11*$^{-/-}$ tails. B. Whole mount *in situ* hybridization in wild type (a, a') and *Gdf11*$^{-/-}$ (b, b') tail buds using a probe for *Tbx6*. Dotted white lines indicate the level of the transversal sections shown in a' and b'. C. Whole mount *in situ* hybridization in wild type (a, a') and *Gdf11*$^{-/-}$ (b, b') tail buds using a probe for *Mesogenin1*. Dotted white lines indicate the level of the transversal

sections shown in a' and b'. Insets show dorsal views of the tail. Grey lines and grey dotted lines depict the contours of each section and the neural tube, respectively. Black arrowheads indicate the ectopic epithelial pocket. D. Whole mount *in situ* hybridization in three wild type (a, c, e; a'', c'',e'') and three *Gdf11*$^{-/-}$ (b, d, f; b', d', f') E10.5 tails using a probe for *Lunatic fringe (Lfng)*. a-f lateral views, a'-f' dorsal views of each corresponding tail bud.

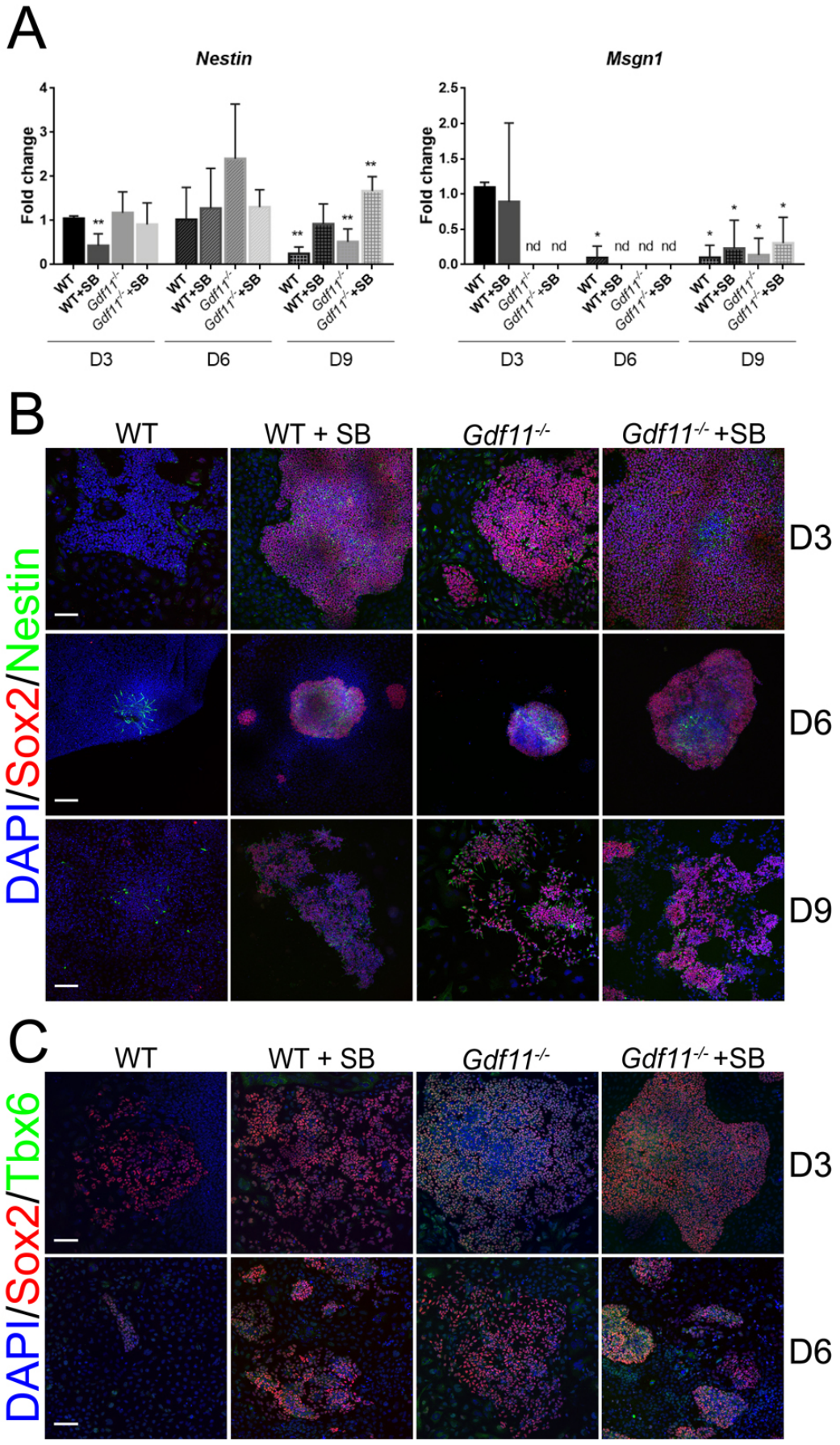
A
Nestin
Msgn1
Fold change
WT
WT+SB
Gdf11-/-
Gdf11-/- +SB
nd
D3
D6
D9
B
WT
WT + SB
Gdf11-/-
Gdf11-/- +SB
DAPI/Sox2/Nestin
C
DAPI/Sox2/Tbx6

Figure S2. Related to Figure 4. Culture of tail bud explants in the presence and absence of Gdf11 signaling. A. RT-qPCR analysis of *Nestin* and *Mesogenin1* (*Msgn1*) expression in explant cultures at day 3 (D3), day 6 (D6), and day 9 (D9) after seeding. Expression in D3 wild type cells was used as the reference to represent relative expression levels obtained in each culture condition of the same time point (*$p<0.05$, **$p<0.01$). Error bars indicate the SD of six independent experiments. n.d. expression not detected . B. Immunofluorescence images of tail bud explants stained for Sox2 and Nestin, or for Sox2 and Tbx6 at the indicated days after seeding. Scale bars: 100μm.

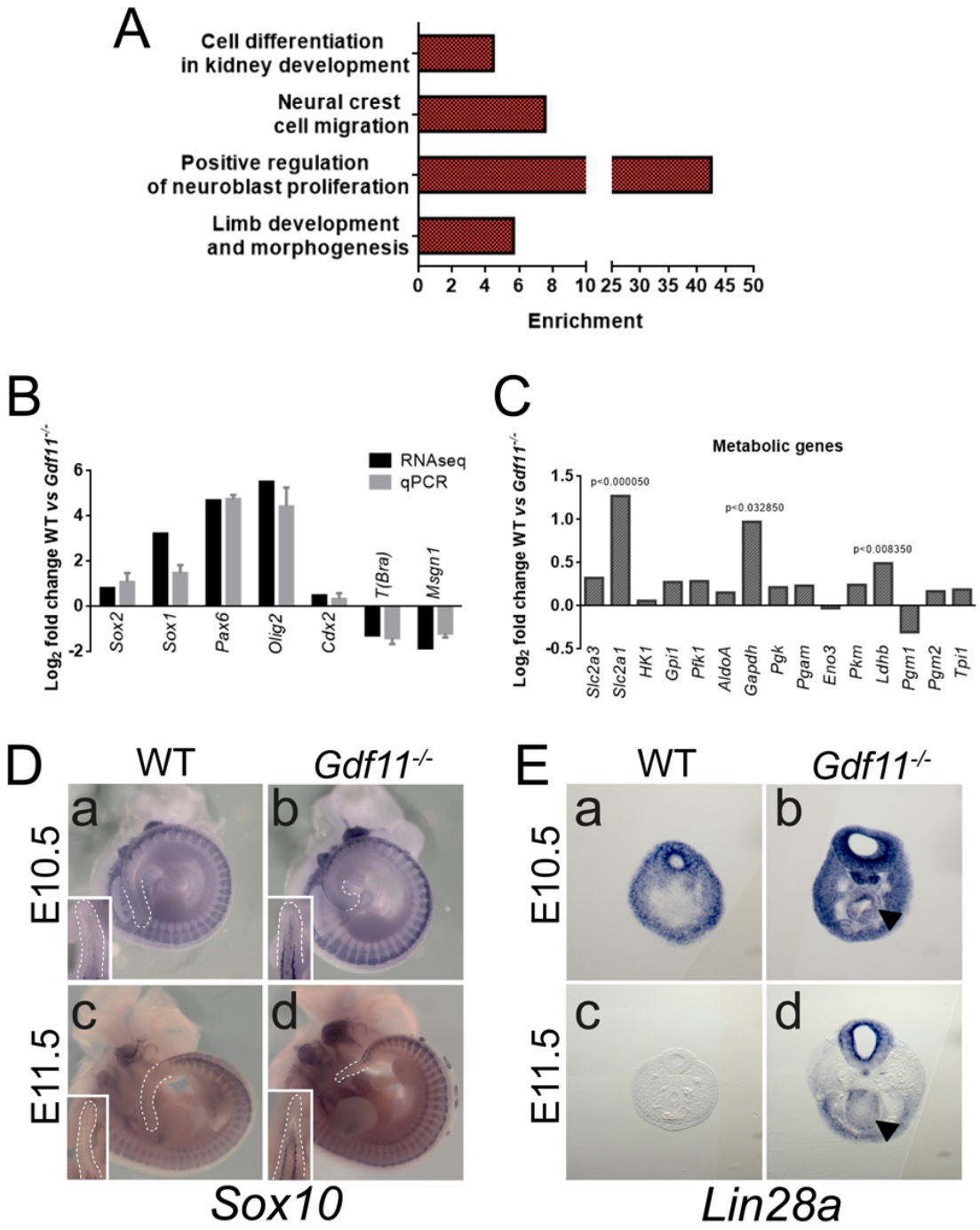

Figure S3. Related to Figure 5. RNA-seq analysis and validation. A. Enrichment analysis of Gene Ontology (GO) terms of 88 genes with a minimum of 2-fold expression change in *Gdf11*$^{-/-}$ *vs* wild type tail buds. B. Expression levels of 7 genes assessed by RT-qPCR in E10.5 wild type and *Gdf11* mutant tail buds compared with the data from the RNA-seq datasets. C. Fold change differences of relevant metabolic genes between wild type and *Gdf11*$^{-/-}$ embryos. D. Whole mount *in situ* hybridization in wild type (a, c) and *Gdf11*$^{-/-}$ (b, d) embryos at E10.5 (a, b) or E11.5 (c, d) using a probe for *Sox10*. Insets show a dorsal view of the tail bud. Dotted lines delimit tail shape. E. Transversal sections of whole mount *in situ* hybridization of wild type (a, c) and *Gdf11*$^{-/-}$ (b, d) embryos at E10.5 (a, b) and E11.5 (c, d) using a probe for *Lin28a*. Black arrowheads indicate the ectopic epithelial pocket.

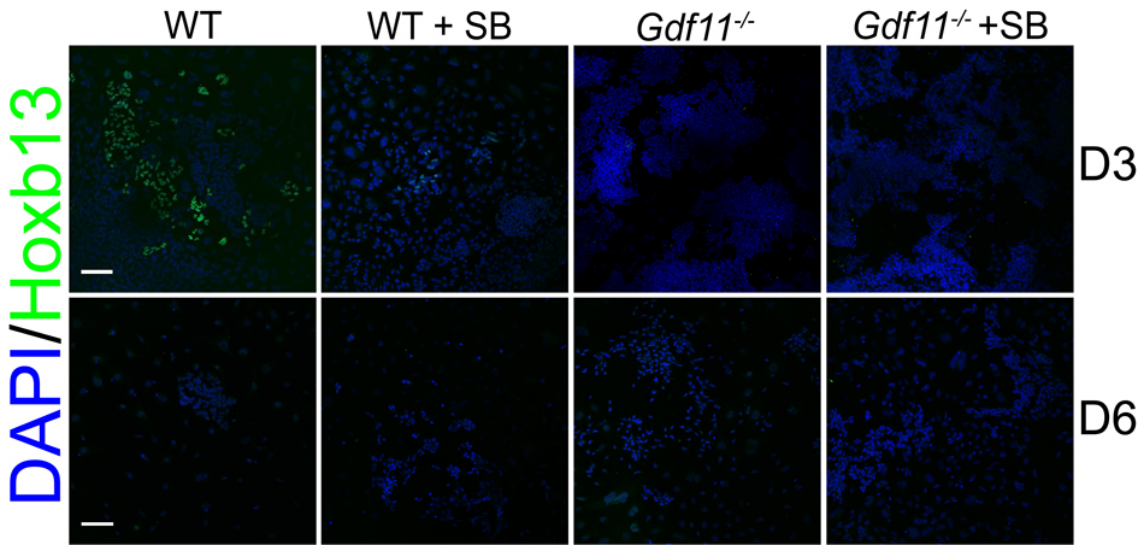

Figure S4. Related to Figure 7. Gdf11 signaling controls the expression of Hoxb13 in tail bud explant cultures. Immunofluorescence images of tail bud explants stained for Hoxb13 at D3 and D6 after plating. Scale bars: 100μm.

Table S1. Related to Figure 5. Comparison of transcript contents in tail buds of E10.5 wild type and Gdf11 mutant embryos.

KEY RESOURCES TABLE

REAGENT or RESOURCE	SOURCE	IDENTIFIER
Antibodies		
Mouse monoclonal anti Hoxb13	Santa Cruz Biotechnology	Cat# sc-28333; RRID:AB_627744
Mouse monoclonal anti Hoxc13	Santa Cruz Biotechnology	Cat# sc-514377
Goat polyclonal anti Lin28a	R & D Systems	Cat# AF3757; RRID:AB_2234537
Mouse monoclonal anti Nestin	Abcam	Cat# ab6142; RRID:AB_305313
Goat polyclonal anti Sox2	Santa Cruz Biotechnology	Cat# sc-17320; RRID:AB_2286684
Rabbit polyclonal anti Sox2	Abcam	Cat# ab92494; RRID:AB_10585428
Goat plyclonal anti T(Bra)	R & D Systems	Cat# AF2085; RRID:AB_2200235
Goat polyclonal anti Tbx6	R & D Systems	Cat# AF4744; RRID:AB_2200834
Rabbit polyclonal Tujl	Abcam	Cat# ab18207 RRID:AB_444319
Donkey anti-goat A488	Thermo Fisher Scientific	Cat# A-11055; RRID:AB_2534102
Donkey anti-goat A647	Thermo Fisher Scientific	Cat# A-21447; RRID:AB_2535864
Donkey anti-mouse A488	Abcam	Cat# ab150105; RRID:AB_2732856
Donkey anti-rabbit A568	Thermo Fisher Scientific	Cat# A10042; RRID:AB_2534017
Rabbit polyclonal anti phospho-Histone 3	Millipore	Cat# 06-570; RRID:AB_310177
Chemicals, Peptides, and Recombinant Proteins		
DAPI	Thermo Fisher Scientific Cat# D3571	RRID: AB_2307445
SB431542	Abcam	Cat # ab120163

Critical Commercial Assays		
In situ cell death kit (TUNEL)	Roche	Cat #11684795910
True-Nuclear™ Transcription Factor Buffer Set	BioLegend	Cat #424401
Deposited Data		
RNA-seq data	NCBI trace and Short-read Archive, accession number SRP167717	N/A
Experimental Models: Organisms/Strains		
Mouse B6;129sv-Gdf11<tm1Sjl>	McPherron et al. 1999	RRID:MGI:3589479
Mouse B6;129S-Hoxc<tm1Nogu>	Suemori and Noguchi, 2000	MGI:3640654
Mouse FVB-Tg(Cdx2-creERT)	Jurberg *et al*, 2013	N/A
Mouse FVB.129S4(B6)-Gt(ROSA)26Sor<tm1Sor>/J	Jackson Labs	Stock No: 09427
Oligonucleotides		
Hoxb13-cDNA-Fwd: CTCGGCTCCCCATGAGCCGATC	This paper	N/A
Hoxb13-cDNA-Rev: GCCGAGTCCTCTGCCAGTCC	This paper	N/A
Lin28a-cDNA-Fwd: ATGGGCTCGGTGTCCAACCAGC	This paper	N/A
Lin28a-cDNA-Rev: TCAATTCTGGGCTTCTGGGAGC	This paper	N/A
Lin28b-cDNA-Fwd: ATGGCCGAAGGCGGGGCAAGC	This paper	N/A
Lin28b-cDNA-Rev: CTAAGTCTTTTTCCGTTTCTG	This paper	N/A
Mesogenin1-cDNA-Fwd: CCAGGAGTCCCCCACTCAAAG	This paper	N/A
Mesogenin1-cDNA-Rev: CAGGTAATTCCGGAGCGTGTG	This paper	N/A

Gdf11-genotyping-Fwd: GCATCCTTTCATGGAGCTTCG	Jurberg et al 2013	N/A
Gdf11-genotyping-WT-Rev: CTGCTGCACCCCTACCAAGATG	Jurberg et al 2013	N/A
Gdf11-genotyping-MUT-Rev: AAAGAACGGAGCCGGTTGG	Jurberg et al 2013	N/A
β-gal-genotyping-Fwd: AGCAGTTTTTCCAGTTCCGTTTATC	This paper	N/A
β-gal -genotyping-Rev: AGCGGCGTCAGAAGTTGTTTTTTAT	This paper	N/A
Cre-ERT-genotyping-Fwd: CGAGTGATGAGGTTCGCAAG	This paper	N/A
CreERT-genotyping-Rev: CCTGATCCTGGCAATTTCGGCT	This paper	N/A
Hoxb13-genotyping-Fwd: ATTCTCTGCTTCCCGTGGAC	This paper	N/A
Hoxb13-genotyping-Rev: ATCTTGCGCCTCTTGTCCTT	This paper	N/A
Hoxc13-genotyping-Fwd: GCCAGCTCCTACCAGGCGATG	This paper	N/A
Hoxc13-genotyping-Rev: CTCTAGCTCCTTCAGCTGCAC	This paper	N/A
Lin28a-genotyping-Fwd: ATGGGCTCGGTGTCCAACCAGC	This paper	N/A
Lin28a-genotyping-Rev: TCAATTCTGGGCTTCTGGGAGC	This paper	N/A
Lin28b-genotyping-Fwd: GAGACGGCAGGATTTACTGATGG	This paper	N/A
Lin28b-genotyping-Rev: CTAAGTCTTTTTCCGTTTCTG	This paper	N/A
Hoxb13-ISH probe-Fwd: AGCCCAGTGTCCAGCACCCTC	This paper	N/A
Hoxb13-ISH probe-Rev: TCACAATCAGCTCAACTCATG	This paper	N/A
Hoxc13-ISH probe-Fwd: CTCCCGCACCCTGTATTGG	This paper	N/A

Hoxc13-ISH probe-Rev: GCCGGTAGCTGCTCACTTCG	This paper	N/A
Lin28a-ISH probe-Fwd: ATGGGCTCGGTGTCCAACCAGC	This paper	N/A
Lin28a-ISH probe-Rev: TCAATTCTGGGCTTCTGGGAGC	This paper	N/A
Lin28b-ISH probe-Fwd: GAGACGGCAGGATTTACTGATGG	This paper	N/A
Lin28b-ISH probe-Rev: CTAAGTCTTTTTCCGTTTCTG	This paper	N/A
Sox2-qPCR-Fwd: TTTGTCCGAGACCGAGAAGC	This paper	N/A
Sox2-qPCR-Rev: CTCCGGGAAGCGTGTACTTA	This paper	N/A
T-qPCR-Fwd: ACCCAGCTCTAAGGAACCAC	This paper	N/A
T-qPCR-Rev: GCTGGCGTTATGACTCACAG	This paper	N/A
Hoxb13-qPCR-Fwd: ATTCTCTGCTTCCCGTGGAC	This paper	N/A
Hoxb13-qPCR-Rev: ATCTTGCGCCTCTTGTCCTT	This paper	N/A
Hoxc13-qPCR-Fwd: AGCACTGGGCTCTTTCCAAT	This paper	N/A
Hoxc13-qPCR-Rev: CTGTAGAGGAACCACGTCTGG	This paper	N/A
Lin28a-qPCR-Fwd: CAACCAGCAGTTTGCAGGTGGCT	This paper	N/A
Lin28a-qPCR-Rev: CCGAACCCCATGCGCACGTT	This paper	N/A

Lin28b-qPCR-Fwd: CAAAGGGAGATAGGTGGAGA	This paper	N/A
Lin28b-qPCR-Rev: GATTCTGCCTCCTGTCTTCC	This paper	N/A
Msgn1-qPCR-Fwd: AGGTAATTCCGGAGCGTGTG	This paper	N/A
Msgn1-qPCR-Rev: TCAAGATGTCTGTCCAGCGG	This paper	N/A
Tbx6-qPCR-Fwd: CACCTTGATTTCACTCCACCC	This paper	N/A
Tbx6-qPCR-Rev: TCCCTCCATTCGCACTAAGG	This paper	N/A
Nestin-qPCR-Fwd: GGGAGATCGCTTAGAGGTG	This paper	N/A
Nestin-qPCR-Rev: ACAGCCAGCTGGAACTTTTC	This paper	N/A
Tubb3-qPCR-Fwd: TGAGGCCTCCTCTCACAAGTA	This paper	N/A
Tubb3-qPCR-Rev: CCGCACGACATCTAGGACTG	This paper	N/A
Pou5f1-qPCR-Fwd: AAGTGGGTGGAGGAAGCCGAC	This paper	N/A
Pou5f1-qPCR-Rev: GGTGTCCCTGTAGCCTCATACTC	This paper	N/A
β-Actin-qPCR-Fwd: ATGAAGATCCTGACCGAGCG	This paper	N/A
β-Actin-qPCR-Rev: TACTTGCGCTCAGGAGGAGC	This paper	N/A
Recombinant DNA		

Cdx2-Lin28a transgenic construct	This paper	N/A
Cdx2-Lin28b transgenic construct	This paper	N/A
Cdx2-Hoxb13 transgenic construct	This paper	N/A
Cdx2-Hoxc13 transgenic construct	Young et al 2009	N/A
Hoxb13-ISH-probe	This paper	N/A
Hoxc13-ISH-probe	This paper	N/A
Lin28a-ISH-probe	This paper	N/A
Lin28b-ISH-probe	This paper	N/A
Msgn1-ISH-probe	This paper	N/A
Sox10-ISH-probe	Britsch *et al*., 2001	N/A
Sox2-ISH-probe	Aires *et al.,* 2016	N/A
T(Bra)-ISH-probe	Aires *et al.,* 2016	N/A
Tbx6-ISH-probe	Hofmann *et al.,* 2004	N/A
Lfng-ISH-probe	Casaca *et al*, 2016	N/A
Software and Algorithms		
Fiji	Fiji	RRID:SCR_002285
GraphPad Prism7	Graphpad Prism	RRID:SCR_002798
FlowJo	FlowJo LLC	RRID:SCR_008520
Other		
VectaShield®	Vector Laboratories Cat# H-1000	RRID:AB_2336789